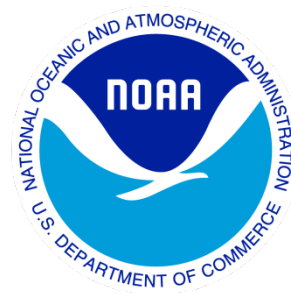

Climate Data Record (CDR) Program

Climate Algorithm Theoretical Basis Document (C-ATBD)

Sea Ice Concentration



CDR Program Document Number: CDRP-ATBD-0107
Configuration Item Number: 01B-11 and 01B-11a
Revision 10 / February 06, 2024

REVISION HISTORY

Rev.	Author	DSR No.	Description	Date
1	Walt Meier, Research Scientist, NSIDC	DSR- 112	Initial release.	09/20/2011
2	Walt Meier, Research Scientist, NSIDC	DSR- 204	Added description of monthly files and memory allocations for processing. Sections 3.2, 3.4.4, and 5.6.	05/29/2012
3	Walt Meier, Research Scientist, NSIDC	DSR- 411	Changes made to describe Version 2 Revision 0 of the CDR. Sections 3.2, 3.3.1, 3.4.1.4, 3.4.4.1, 3.4.4.2, and 5.6. 6.1.4 (deleted)	03/26/2013
4	Ann Windnagel, Professional Research Assistant, NSIDC	DSR- 920	Changes made to describe Version 2 Revision 1 of the CDR. Updated Figures 2 and 5 in Section 3.2, Sections 1.3 and 5.6, and Table 12.	09/19/2015
5	Ann Windnagel, Professional Research Assistant, NSIDC	DSR- 1148	Changes made to describe Version 3 and the near-real-time portion of the time series: Updated sections 1.1, 2.1, 2.2, 3, 4, 5.6, 6, and 8.	09/14/2017
6	Ann Windnagel, Professional Research Assistant, NSIDC	DSR- 1216	Changes made to describe Version 3 Revision 1. Updated sections 3.2, 3.3, and 3.4. Changes made to address Version 3.1: Updated section 3.3.1.	12/20/2017
7	Ann Windnagel, Professional Research Assistant, NSIDC	DSR- 1240	Changes made to tables 3, 4, and 5: instruments for the input data were changed from SMMIS and SMM/I to SSMIS and SSM/I.	03/06/2018
8	Ann Windnagel, Professional Research Assistant, NSIDC	DSR- 1525	Made major updates to the entire document to reflect the new Version 4 TCDR and Version 2 ICDR release.	04/19/2021
9	Ann Windnagel, Professional Research Assistant, NSIDC	DSR- 1527	Minor revision due to typographical errors	06/03/2021
10	Ann Windnagel, Professional Research Assistant, NSIDC	DSR- 1528	Major revision of entire document to reflect changes with the new Version 5 Enhanced TCDR and ICDR	01/31/2023

TABLE of CONTENTS

1. INTRODUCTION	6
1.1 Purpose	6
1.2 Definitions.....	6
1.3 Referencing this Document.....	7
1.4 Document Maintenance	7
2. OBSERVING SYSTEMS OVERVIEW.....	7
2.1 Products Generated.....	7
2.2 Instrument Characteristics	7
3. ALGORITHM DESCRIPTION.....	10
3.1 Algorithm Overview	10
3.2 Processing Outline	10
3.2.1 Daily Processing	12
3.2.2 Monthly Processing.....	14
3.3 Algorithm Input.....	14
3.3.1 Primary Sensor Data.....	14
3.3.2 Ancillary Data	16
3.4 Theoretical Description	17
3.4.1 Physical and Mathematical Description	18
3.4.2 Data Merging Strategy	34
3.4.3 Algorithm Output	35
4. TEST DATASETS AND OUTPUTS	47
4.1 Test Input Datasets	47
4.2 Test Output Analysis	47
4.2.1 Reproducibility.....	47
4.2.2 Precision and Accuracy.....	47
4.2.3 Error Budget.....	48
5. PRACTICAL CONSIDERATIONS.....	49
5.1 Numerical Computation Considerations	49
5.2 Programming and Procedural Considerations.....	49
5.3 Quality Assessment and Diagnostics.....	49
5.4 Exception Handling	50
5.5 Algorithm Validation and Error Assessment	50
5.5.1 Errors from sensor characteristics and gridding scheme.....	51
5.5.2 Errors due to surface variation and ambiguities.....	53
5.5.3 Errors due to atmospheric effects	54
5.5.4 Summary of error sources and magnitudes.....	55
5.6 Processing Environment and Resources	55
5.6.1 Look-Up Table Description.....	56
6. ASSUMPTIONS AND LIMITATIONS.....	57
6.1 Algorithm Performance	58

6.2	Sensor Performance	58
7.	FUTURE ENHANCEMENTS	59
7.1.1	Improved Resolution Matching Between SMMR-SSMI-SSMIS and AMSR-E/AMSR2	59
7.1.2	Reprocessing Using a New Version of Brightness Temperatures.....	59
7.1.3	EASE-Grid 2.0 Version of Sea Ice CDR	59
7.1.4	New Algorithm Coefficients for Calibration	60
7.1.5	Improved Pole-Hole Filling.....	60
7.1.6	Fill Remaining Temporal Gaps Using Statistical Modeling	60
8.	REFERENCES	60
	APPENDIX A - ACRONYMS AND ABBREVIATIONS	66

LIST of FIGURES

Figure 1: Flowchart showing the overview of sea ice concentration TCDR processing. Note that the ICDR processing is identical except that the input data is the LANCE AMSR2 data.....	11
Figure 2: Overview of main python code for the daily sea ice concentration TCDR processing. Note that the ICDR processing is identical except that the input data is LANCE AMSR2 data.....	12
Figure 3: Overview of the TCDR Bootstrap and NASA Team processing code.....	13
Figure 4: Monthly TCDR processing.....	14
Figure 5: Sample plot of GR vs. PR with typical clustering of grid cell values (small dots) around the 0% ice (open water) point (blue star) and the 100% ice line (circled in red). First year (FY) ice clusters at the top of the 100% ice line, and multi-year (MY) ice clusters at the bottom. Points with a mixture of ice and water (circled in green) fall between these two extremes. Adapted from Figure 10-2 of Steffen et al. (1992).....	19
Figure 6: Example of the relationship of the 19V vs. 37V T_B (in Kelvin) used in the Bootstrap algorithm. Brightness temperatures typically cluster around the line segments AD (representing 100% sea ice) and OW (representing 100% open water). For points that fall below the AD-5 line (dotted line), bootstrap uses T_B relationships for 37H vs. 37V. Adapted from Comiso and Nishio (2008).	22
Figure 7. A comparison of sea ice concentration off the NE coast of Greenland for 30 July 2021 for the 25 km SSMIS (A), 12.5 km AMSR2 (B), and 500 m MODIS visible band image (C) sensors. This close-up view shows the better ice edge delineation from AMSR2 over SSMIS to capture features in the ice pack that are visible in the MODIS image. The lower	

resolution SSMIS image “smears” the ice edge over the larger 25 km x 25 km grid cells.26

Figure 8. This image, showing Ellesmere Island and the NW coast of Greenland, highlights the difference of coastal areas between the 12.5 km grids and the 25 km grids. Areas that are ocean in both grids are blue. Areas that are not surrounded by enough ocean pixels for bilinear interpolation to work are green. Areas that are ocean in the 12.5 km grids but are land in the 25 km grids are red. Areas that are land in both grids are black.27

Figure 9. Arctic Pole Hole: Tan grid cells are where there is never any data. Red cells are where data occasionally occur.30

Figure 10: Sample scatter plot of 19V vs. (22V-19V) (left) and 19V vs. 37V (right) T_{BS} from SSM/I. Values shaded in blue around the OW segment are masked to 0% concentration. From Comiso and Nishio (2008).....31

Figure 11: Schematic of grid cell values used in calculation of the CDR standard deviation field. All non-missing ocean/sea ice concentration values (C), from both the NASA Team and Bootstrap algorithm, of the 3 x 3 box surrounding each (I,J) grid cell (up to 18 total values) are used to calculate the standard deviation. A minimum of six grid cells with valid values is used as a threshold for a valid standard deviation.....42

LIST of TABLES

Table 1: Comparison of Nimbus, DMSP, Aqua, and GCOM-W1 orbital parameters 8

Table 2: Instrument characteristics of SMMR, SSM/I, SSMIS, AMSR-E, and AMSR2 and frequencies used in the SIC CDR algorithm (Gloersen and Barath, 1977; Hollinger et al., 1990; Kunkee et al., 2008; T. Kawanishi *et al.*, 2003; Nakagawa, 2010) 9

Table 3: Temporal range of the instruments used for the input brightness temperatures for the sea ice ECDR variable.15

Table 4. Arctic Pole Hole Sizes by Instrument17

Table 5: NASA Team tie-point values (in Kelvin) for each sensor.....22

Table 6. GR3719 and Gr2219 criteria by instrument and hemisphere31

Table 7: List of flag values used in the daily CDR QA field. A grid cell that satisfies more than one criteria will contain the sum of all applicable flag values.....39

Table 8. Spatial interpolation flag values. A grid cell that satisfies more than one criteria will contain the sum of all applicable flag values.40

Table 9: List of flag values used in the monthly CDR QA bit mask. A grid cell that satisfies more than one criteria will contain the sum of all applicable flag values. For example, if spatial interpolation was performed and melt detected then the value will be 160 (32 + 128).45

Table 10: Possible error sources and magnitudes for the sea ice CDR.....49

Table 11: List of error sources and typical error magnitudes in % concentration for the NASA Team (NT) and Bootstrap (BT) algorithms with biases and typical regimes.55

Table 13. ECDR Ancillary Files Content Description.....57

1. Introduction

1.1 Purpose

The purpose of this document is to describe the sea ice concentration (SIC) climate data record (CDR) algorithm (Meier et al. 2014; Peng et al. 2013). Beginning in 2015, updates are submitted to the National Centers for Environmental Information (NCEI) by Florence Fetterer at the National Snow and Ice Data Center (NSIDC).

The SIC CDR algorithm is used to create sea ice concentrations from passive microwave data from the Scanning Multichannel Microwave Radiometer (SMMR) on the Nimbus 7 satellite, the Special Sensor Microwave/Imager (SSM/I) and the Special Sensor Microwave Imager and Sounder (SSMIS) sensors on U.S. Department of Defense Meteorological Satellite Program (DMSP) platforms, the Advanced Microwave Scanning Radiometer - Earth Observing System Sensor (AMSR-E) sensor on Aqua, and the Advanced Microwave Scanning Radiometer 2 (AMSR2) sensor on GCOM-W1. The goal of the SIC CDR is to provide a consistent, reliable, and well-documented product that meets CDR guidelines as defined in *Climate Data Records from Environmental Satellites* (NAS, 2004). Previously, this product was supplied in two parts. A final (TCDR) product called the *NOAA/NSIDC Climate Data Record of Passive Microwave Sea Ice Concentration* (<https://nsidc.org/data/g02202/versions/4>), and a near-real-time (ICDR) provisional called the *Near-Real-Time NOAA/NSIDC Climate Data Record of Passive Microwave Sea Ice Concentration* (<https://nsidc.org/data/g10016/versions/2>). With the release of version 5, both the TCDR and ICDR will be part of the same data set (<https://nsidc.org/data/g02202/versions/5>). The ICDR product will be the most recent two or three weeks of data. Note that the CDR V5 improves the resolution of the product from a 25 km grid to a 12.5 km grid. Because of this improvement, it is sometimes referred to as the enhanced CDR (ECDR) in this document.

The algorithm is defined in the computer program (code) that accompanies this document; and thus, the intent here is to provide a guide to understanding that algorithm, from both a scientific perspective and a software engineering perspective to assist in evaluation of the code.

1.2 Definitions

The following is a summary of the symbols used to define the algorithm.

$$T_B = \text{brightness temperature} = \varepsilon * T \quad (1)$$

$$\varepsilon = \text{emissivity} \quad (2)$$

$$T = \text{physical temperature} \quad (3)$$

$$PR = \text{polarization ratio} \quad (4)$$

$$GR = \text{gradient ratio} \quad (5)$$

1.3 Referencing this Document

This document should be referenced as follows:

Sea Ice Concentration - Climate Algorithm Theoretical Basis Document, NOAA Climate Data Record Program CDRP-ATBD-0107 Rev. 10 (2024).

1.4 Document Maintenance

This is the ATBD for the Sea Ice Concentration Climate Data Record, Version 5, Revision 0.

2. Observing Systems Overview

2.1 Products Generated

The primary generated product is the SIC CDR based on gridded brightness temperatures (T_{BS}) from the Nimbus-7 SMMR, the DMSP series of SSM/I and SSMIS, and the AMSR-E and AMSR2 series of passive microwave radiometers. These data are an estimate of sea ice concentration that are produced by combining concentration estimates from two algorithms developed at the NASA Goddard Space Flight Center (GSFC): the NASA Team algorithm (Cavalieri et al., 1984) and the Bootstrap algorithm (Comiso, 1986). These algorithms are described in more detail in Section 3. NSIDC uses each individual algorithm to process and combine gridded brightness temperatures from SMMR, SSM/I, and SSMI data acquired from NASA Goddard Space Flight Center (GSFC) and gridded brightness temperatures from AMSR-E/AMSR2 data acquired from Japan Aerospace Exploration Agency (JAXA). See Section 3.3 for more information on the input brightness temperatures.

Accompanying the concentration estimates are data quality information fields. One field is a concentration standard deviation that indicates local spatial variability. Grid cells with high standard deviations indicate values with lower confidence levels. Another field includes quality information such as melt state and proximity to the coast, regimes that tend to have higher errors.

2.2 Instrument Characteristics

An overview of the instruments used in the generation of the SIC CDR, along with the pertinent channels and frequencies, is listed in Table 2. A brief description of each instrument is given in this section.

The SMMR passive microwave sensor was launched aboard the Nimbus-7 satellite in October 1978. The SMMR sensor was a ten-channel sensor that measured orthogonally polarized (horizontal (H) and vertical (V)) antenna temperature data in five microwave frequencies (Gloersen and Hardis, 1978). Only 5 of these are used in the

creation of the SIC CDR: 18.0 (V/H), 21.0 (V), and 37.0 (V/H) GHz. The NASA Nimbus-7 SMMR sensor, which predates DMSP, extends the total time series to late 1978 with every-other-day concentration estimates.

The first SSM/I sensor was launched aboard the DMSP-F8 mission in 1987 (Hollinger et al., 1990). A series of SSM/I conically-scanning sensors on subsequent DMSP satellites has provided a continuous data stream since then. However, only SSM/I sensors on the DMSP-F8, -F11, and -F13 platforms are used in the generation of the CDR. The SSM/I sensor has seven channels at four frequencies. The ones used in the SIC CDR processing are the 19.4 (V/H), 37.0 (V/H), and 22.2 (V) GHz.

Beginning with the launch of F16 in 2003, the SSM/I sensor was replaced by the SSMIS sensor. The SSMIS sensor has 24 channels (Kunkee et al., 2008) but the same 19.4 (V/H), 22.2 (V), and 37.0 (V/H) GHz channels are used in the generation of the SIC CDR. Only the F17 SSMIS instrument is used for SIC CDR processing.

AMSR-E was launched aboard the Aqua satellite on 4 May 2002 with 12 channels. AMSR2 was launched aboard GCOM-W1 on 18 May 2012 with 16 channels. Both instruments have channel frequencies similar to those of the SMMR, SSM/I, and SSMIS instruments. The AMSR-E and AMSR2 channels used to process the SIC CDR are the 18.7 (V/H), 23.8 (V), and 36.5 (V/H) GHz channels.

For simplicity in this document, the channels are denoted as simply 19 (V/H) for the 18.0/18.7/19.4 GHz channels, 22V for the 21.0/22.2/23.8 GHz channels, and 37 (V/H) for the 36.5/37.0 GHz channels. Depending on the platform, the satellite altitudes are 700 km to 955 km and sensor (earth incidence) angles are 50.2° to 55.0° (Table 1).

Satellite	Launch Date (YYYY-MM-DD)	Nominal Altitude (km)	Inclination Angle (degrees)	Orbital Period (minutes)	Ascending Node Equatorial Crossing Time at Launch (approximate local time to the nearest half hour)
Nimbus-7	1978-10-24	955	99.1	104	12:00
DMSP-F8	1987-06-18	860	98.8	102	06:00
DMSP-F11	1991-11-28	830	98.8	101	17:30
DMSP-F13	1995-03-24	850	98.8	102	17:30
DMSP-F17	2006-11-04	855	98.8	102	17:30
Aqua	2002-05-04	705	98.2	98.8	13:30
GCOM-W1	2012-05-18	700	98.2	98.8	13:30

Table 1: Comparison of Nimbus, DMSP, Aqua, and GCOM-W1 orbital parameters

A polar orbit and wide swath provide near-complete coverage at least once per day in the polar regions except for a small region around the North Pole called the pole hole. The footprint or instantaneous field of view (IFOV) of the sensor varies with frequency (Table 2). Regardless of footprint size, the channels are gridded onto a 12.5 km polar stereographic grid.

Satellite	Sensor	Frequencies (GHz)	IFOV (km)	Swath Width (km)	Earth Incidence Angle (degrees)
NIMBUS-7	SMMR	18.0	55 x 41	783	50.2
		21.0	46 x 30		
		37.0	27 x 18		
DMSP-F8	SSM/I	19.4	69 x 43	1400	53.1
		22.2	60 x 40		
		37.0	37 x 28		
DMSP-F11	SSM/I	19.4	69 x 43	1400	52.8
		22.2	60 x 40		
		37.0	37 x 28		
DMSP-F13	SSM/I	19.4	69 x 43	1400	53.4
		22.2	60 x 40		
		37.0	37 x 28		
DMSP-F17	SSMIS	19.4	72 x 44	1700	53.1
		22.2	72 x 44		
		37.0	44 x 26		
Aqua	AMSR-E	18.7	16 x 27	1450	55.0
		23.8	18 x 32		
		36.5	8 x 14		
GCOM-W1	AMSR2	18.7	14 x 22	1450	55.0
		23.8	15 x 26		
		36.5	7 x 12		

Table 2: Instrument characteristics of SMMR, SSM/I, SSMIS, AMSR-E, and AMSR2 and frequencies used in the SIC CDR algorithm (Gloersen and Barath, 1977; Hollinger et al., 1990; Kunkee et al., 2008; T. Kawanishi *et al.*, 2003; Nakagawa, 2010)

3. Algorithm Description

3.1 Algorithm Overview

The Sea Ice Concentration CDR algorithm uses concentration estimates derived at NSIDC from the NASA Team (Cavalieri et al., 1984) and Bootstrap (Comiso, 1986) algorithms as input data and merges them into a combined single concentration estimate based on the known characteristics of the two algorithms. First, the Bootstrap 10% concentration threshold is used as a cutoff to define the limit of the ice edge. Second, within the ice edge, the higher of the two concentration estimates from the NASA Team and Bootstrap algorithms is used for the CDR input value. The reason for these two approaches is discussed further in Section 3.4.1.3. Automated quality control measures are implemented independently on the NASA Team and Bootstrap outputs. Two weather filters, based on ratios of channels sensitive to enhanced emission over open water, are used to filter weather effects. The NASA Team 2 land-spillover correction is used to filter out much of the error due to mixed land-ocean grid cells. Finally, invalid ice masks are applied to screen out errant retrievals of ice in regions where sea ice never occurs.

3.2 Processing Outline

The following flow diagram (Figure 1) describes the general processing for the finalized daily and monthly TCDR sea ice concentrations and the near-real-time provisional daily and monthly ICDR sea ice concentrations.

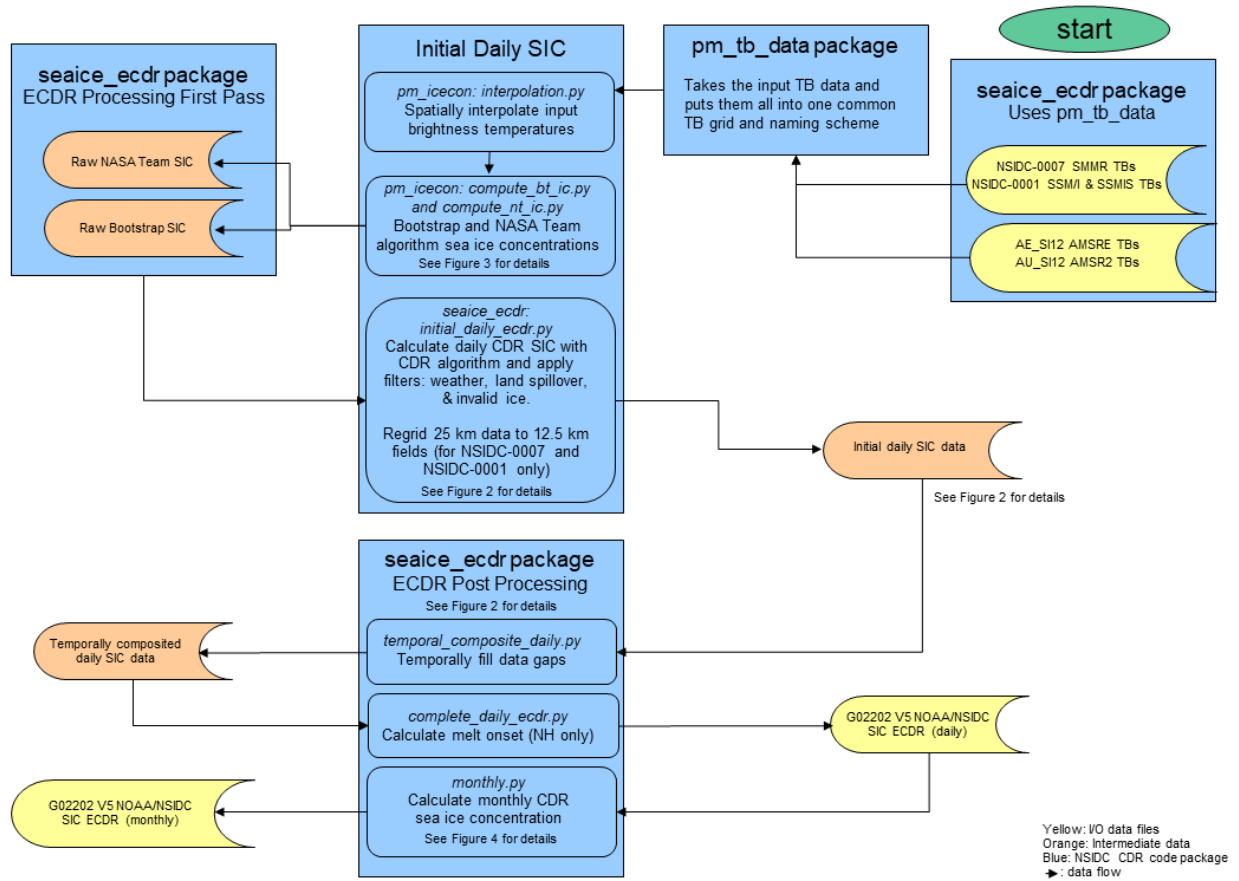


Figure 1: Flowchart showing the overview of sea ice concentration TCDR processing. Note that the ICDR processing is identical except that the input data is the LANCE AMSR2 data.

3.2.1 Daily Processing

The following flow diagrams (Figure 2 and Figure 3) describe the processing of the daily CDR sea ice concentration in detail.

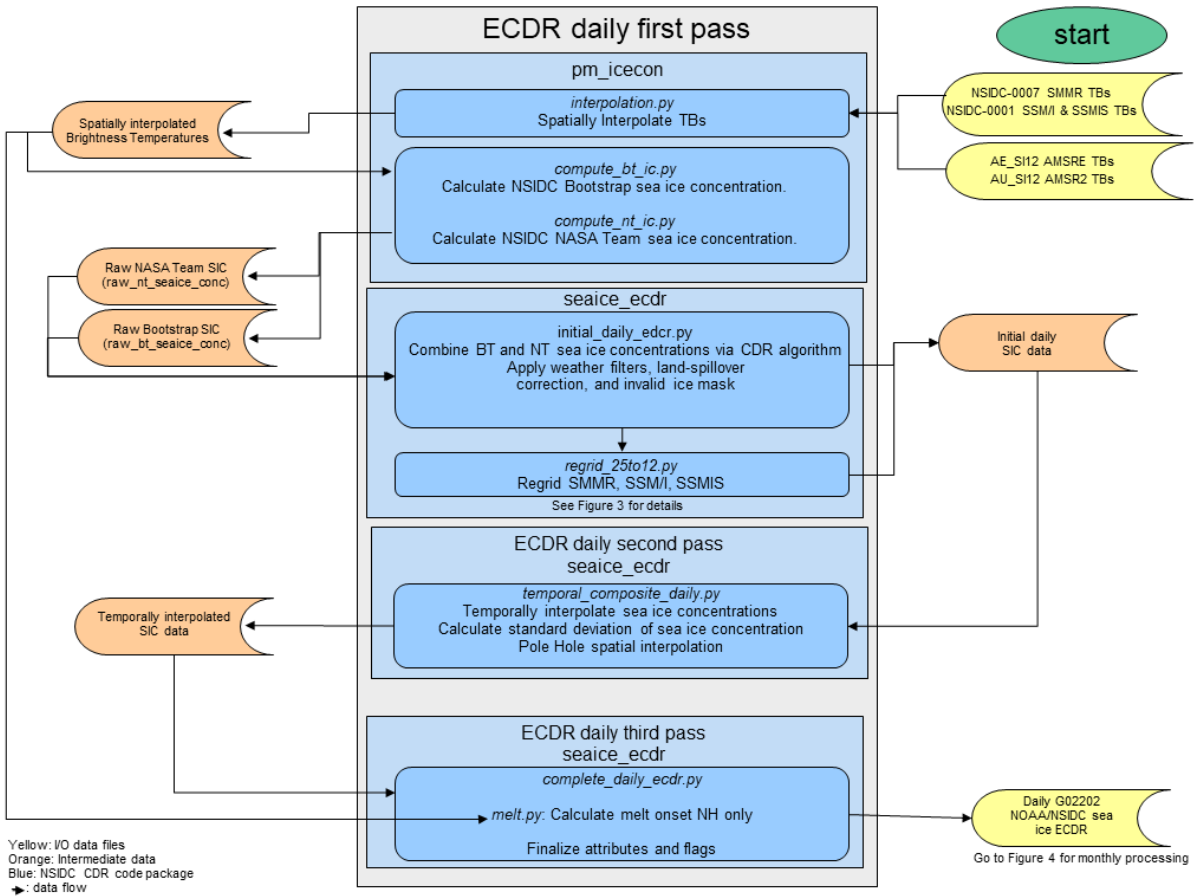


Figure 2: Overview of main python code for the daily sea ice concentration TCDR processing. Note that the ICDR processing is identical except that the input data is LANCE AMSR2 data.

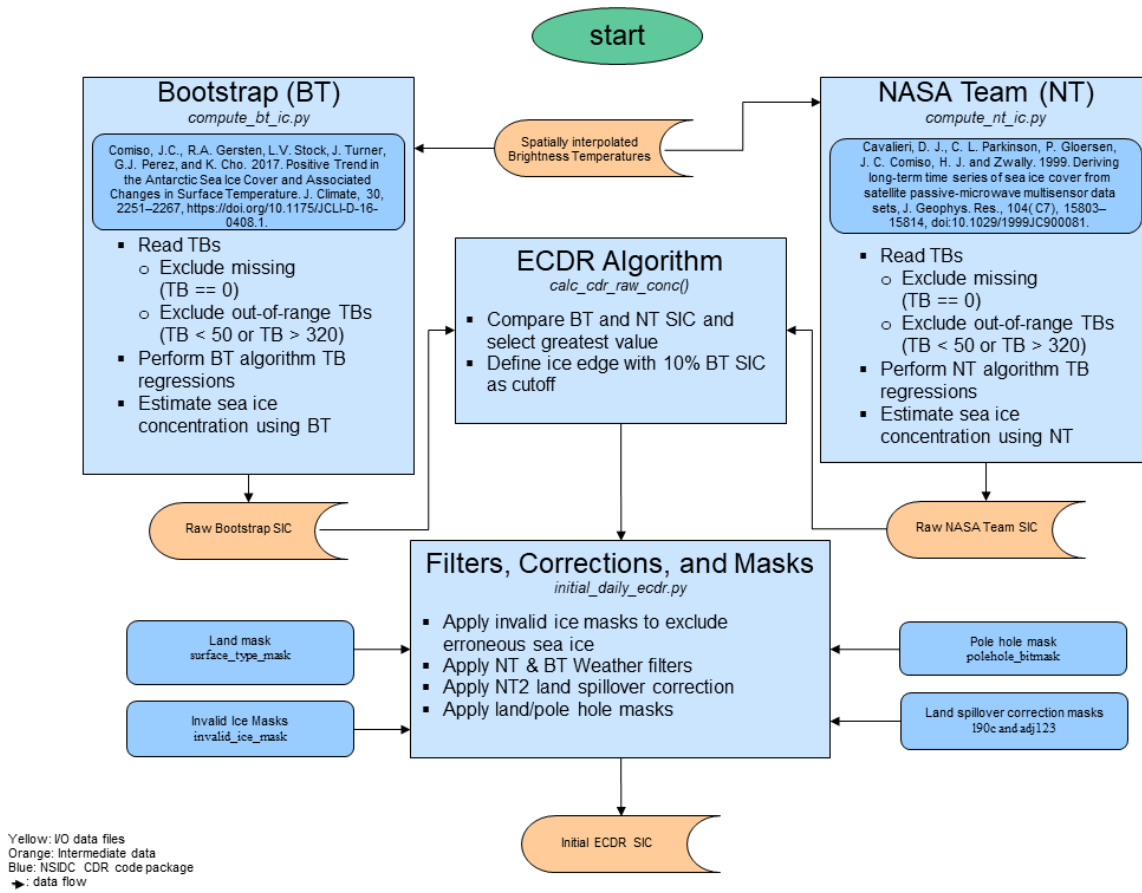


Figure 3: Overview of the TCDR Bootstrap and NASA Team processing code.

3.2.2 Monthly Processing

The following flow diagram (Figure 4) describes the processing of the monthly CDR sea ice concentration for the finalized TCDR data and the near-real-time ICDR data.

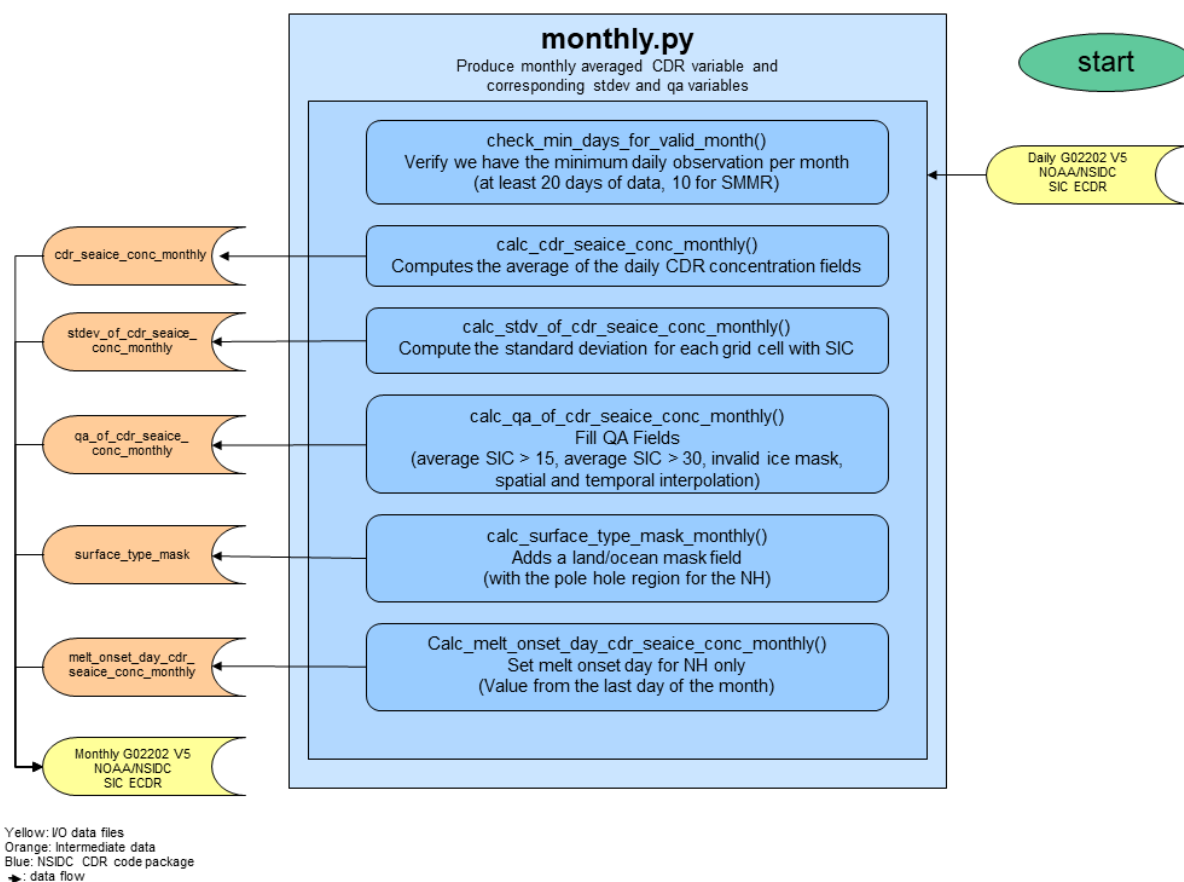


Figure 4: Monthly TCDR processing.

3.3 Algorithm Input

3.3.1 Primary Sensor Data

Calibrated and gridded brightness temperatures from Nimbus-7 SMMR, DMSP SSM/I, DMSP SSMIS, Aqua AMSR-E, and GCOM-W1 AMSR2 passive microwave sensors are used as the primary input data for this sea ice concentration CDR. See Table 3 for a list of the sensors and their dates and Table 2 for a list of channels used. The rationale for using only these satellites was made to keep the equatorial crossing times as consistent

as possible to minimize potential diurnal effects from data on sun-synchronous orbits of the satellites.

Sensor	Temporal Range	Product	Input Data Product
GCOM-W1 AMSR2	Near-real-time (present – two weeks prior)	ICDR	https://cmr.earthdata.nasa.gov/search/concepts/C1886605827-LANCEAMSR2.html
GCOM-W1 AMSR2	03 Jul 2012 – two weeks prior	TCDR	https://nsidc.org/data/au_si12
DMSP-F17 SSMIS	04 Oct 2011 – 02 Jul 2021	TCDR	https://nsidc.org/data/nsidc-0001
Aqua AMSR-E	01 Jun 2002 – 03 Oct 2011	TCDR	https://nsidc.org/data/ae_si12
DMSP-F13 SSM/I	01 Oct 1995 – 31 May 2002	TCDR	https://nsidc.org/data/nsidc-0001
DMSP-F11 SMM/I	03 Dec 1991 – 30 Sep 1995	TCDR	https://nsidc.org/data/nsidc-0001
DMSP-F8 SSM/I	10 Jul 1987 – 02 Dec 1991 Note: There are no data from 3 December 1987 through 12 January 1988 due to satellite problems.	TCDR	https://nsidc.org/data/nsidc-0001
Nimbus-7 SMMR	25 October 1978 – 09 Jul 1987	TCDR	https://nsidc.org/data/nsidc-0007

Table 3: Temporal range of the instruments used for the input brightness temperatures for the sea ice ECDR variable.

The AMSR-E and AMSR2 swath data are gridded onto a daily composite 12.5 km polar stereographic grid using a drop-in-the-bucket method. The SMMR, SSM/I, and SSMIS are gridded onto a daily composite 25 km polar stereographic grid using a drop-in-the-bucket method. For each grid cell, all footprints from all passes each day whose centers fall within the grid cell are averaged together. Thus, some grid cells may be an average of several (4 or 5) passes during a given day and some may be from only one pass. Note that the polar stereographic grid is not equal area; the latitude of the true scale (tangent of the planar grid) is 70 degrees. The Northern Hemisphere 12.5 km grid is 608 columns by 896 rows, and the Southern Hemisphere grid is 632 columns by 664 rows. Further information on the polar stereographic grid used at NSIDC can be found on the NSIDC web site on the Polar Stereographic Projection and Grid web page (<https://nsidc.org/data/user-resources/help-center/guide-nsidcs-polar-stereographic-projection>).

The passive microwave channels employed for the sea ice concentration product are the 19 (V/H), 22 (V), and 37 (V/H) GHz frequencies. The NASA Team algorithm uses the 19 GHz H and V channels and the 37 GHz V channel. The 22 GHz V channel is

used with the 19 GHz V channel for one of the weather filters. The Bootstrap algorithm uses 37 GHz H and V channels and the 19 GHz V channel; it also uses the 22 GHz V channel for a weather filter.

3.3.2 Ancillary Data

Ancillary data required to run the NASA team and Bootstrap algorithms: (A) surface type masks, (B) invalid sea ice masks to define the limits of possible sea ice, (C) a land adjacency mask that indicates ocean grid cells that are near land, (D) an expected land spillover effect mask (for the NASA Team 2 land-spillover correction), (E) a pole hole mask. Section 5.6.1 describes the files that contain these ancillary data.

- A. The surface type mask provides a mask of land surface types: ocean, lake, coast, and land.
- B. Invalid ice ocean climatology masks are used to remove any remaining spurious ice not filtered by automated corrections in regions where sea ice is not possible. There are monthly masks for each hemisphere. For the Northern Hemisphere, remaining spurious ice is removed using the Polar Stereographic Valid Ice Masks Derived from National Ice Center Monthly Sea Ice Climatologies. There are 12 masks, one for each month. They are available from NSIDC (<https://nsidc.org/data/nsidc-0622>). The Southern Hemisphere masks, produced from information from Goddard, are found in the ancillary directory in the code base that is available for download from the NOAA NCEI CDR program (<https://www.ncei.noaa.gov/products/climate-data-records/sea-ice-concentration>). In addition, there are also daily climatology ice masks for the SMMR sensor derived from Bootstrap Sea Ice Concentrations for both the Northern and Southern hemispheres. These masks are discussed further in Section 3.4.1.5.

In order to reduce the inclusion of clearly false-positive ice concentration values, two invalid ice masks are applied to all data. One is a monthly climatology ice mask and the other is a daily climatology ice mask. In the Northern Hemisphere, the monthly ice mask comes from NSIDC-0622. In the Southern Hemisphere, the monthly masks are derived from the Goddard NASA Team algorithm NSIDC-0051. For both hemispheres, the daily mask is derived from the Goddard Bootstrap algorithm NSIDC-0079 data and is only applied to the CDR sea ice concentration. Ocean cells that are not valid sea ice locations are set to 0% concentration.

- C. A mask that indicates whether ocean grid cells are 1, 2, 3, or >3 pixels away from land.
- D. Because of the large instantaneous field of view of the passive microwave sensors, mixed land-ocean grid cells occur. These present a problem for the automated concentration algorithm because the emission from the combined land-ocean region has a signature similar to sea ice and is interpreted as such by

the algorithms. We use the NASA Team 2 (NT2) land spillover correction to filter out this false ice. For the NT2 algorithm, a filtering mechanism has been implemented to automatically remove much of these false coastal ice grid cells by using the land adjacency mask (C) and a mask that estimates how land might look if it was interpreted as sea ice. This estimate is calculated by assuming that nearby ocean pixels are 0% sea ice concentration and nearby land grid cells are 90% sea ice concentration and computing the average of grid cells near each point.

- E. In the Northern Hemisphere, there are grid cells near the pole where observations are not possible because of the shape of the satellite's orbit. A pole hole mask file has been generated for each sensor so that these unobserved locations can be treated differently than other missing data. See Table 4 for a list of the sizes of these holes. In this data product, the pole hole is filled where possible. See Section 3.4.1.5 for a description of how this filling is done.

Sensor	Arctic pole hole Area (million km ²)	Minimum Latitude
SMMR	1.193	84.12° N
SSM/I F08	0.318	86.72° N
SSM/I F11	0.318	86.72° N
SSM/I F13	0.318	86.72° N
SSMIS F17	0.0292	89.02° N
AMSR-E	0.0341	88.94° N
AMSR2	0.0286	89.07° N

Table 4. Arctic Pole Hole Sizes by Instrument

3.4 Theoretical Description

Passive microwave radiation is naturally emitted by the Earth's surface and overlying atmosphere. This emission is a complex function of the microwave radiative properties of the emitting body (Hallikainen and Winebrenner, 1992). However, for the purposes of microwave remote sensing, the relationship can be described as a simple function of the physical temperature (T) of the emitting body and the emissivity (ϵ) of the body.

$$T_B = \epsilon * T \quad (6)$$

T_B is the brightness temperature and is the parameter (after calibrations) retrieved by satellite sensors and is the input parameter to passive microwave sea ice concentration algorithms.

3.4.1 Physical and Mathematical Description

The microwave electromagnetic properties of sea ice are a function of the physical properties of the ice, such as crystal structure, salinity, temperature, or snow cover. In addition, open water typically has an electromagnetic emission signature that is distinct from sea ice emission (Eppler et al., 1992). These properties form the basis for passive microwave retrieval of sea ice concentrations.

Specifically, the unfrozen water surface is highly reflective in much of the microwave regime, resulting in low emission. In addition, emission from liquid water is highly polarized. When salt water initially freezes into first-year (FY) ice (ice that has formed since the end of the previous melt season), the microwave emission changes substantially; the surface emission increases and is only weakly polarized. Over time as freezing continues, brine pockets within the sea ice drain, particularly if the sea ice survives a summer melt season when much of the brine is flushed by melt water. This multi-year (MY) ice has a more complex signature with characteristics generally between water and FY ice. Other surface features can modify the microwave emission, particularly snow cover, which can scatter the ice surface emission and/or emit radiation from within the snowpack. Atmospheric emission also contributes to any signal received by a satellite sensor. These issues result in uncertainties in the retrieved concentrations, which are discussed further below.

Because of the complexities of the sea ice surface as well as surface and atmospheric emission and scattering, direct physical relationships between the microwave emission and the physical sea ice concentration are not feasible. Thus, the standard approach is to derive concentration through empirical relationships. These empirically-derived algorithms take advantage of the fact that brightness temperature in microwave frequencies tend to cluster around consistent values for pure surface types (100% water or 100% sea ice). Concentration can then be derived using a simple linear mixing equation (Zwally et al., 1983) for any brightness temperature that falls between the two pure surface values:

$$T_B = T_I C_I + T_O (1 - C_I) \quad (7)$$

Where T_B is the observed brightness temperature, T_I is the brightness temperature for 100% sea ice, T_O is the brightness temperature for open water, and C_I is the sea ice concentration.

In reality, such an approach is limited by the surface ambiguities and atmospheric emission. Using combinations of more than one frequency and polarization limits these effects, resulting in better discrimination between water and different ice types and a more accurate concentration estimate.

There have been numerous algorithms derived using various combinations of the frequencies and polarizations on the SMMR and SSM/I sensors. Two commonly used algorithms are the NASA Team (Cavalieri et al., 1984) and Bootstrap (Comiso, 1986),

both developed at NASA GSFC. The sea ice concentration CDR described here is produced via a combination of estimates from the NASA Team algorithm and the Bootstrap algorithm. Below, each algorithm is described in more detail followed by a description of quality control (QC) procedures and the procedure to merge the two algorithm estimates into the final CDR product with the sea ice concentration CDR algorithm.

3.4.1.1 NASA Team Algorithm

The NASA Team algorithm uses brightness temperatures from the 19V, 19H, and 37V channels (Cavalieri et al., 1984). The methodology is based on two brightness temperature ratios, the polarization ratio (PR) and spectral gradient ratio (GR), as defined below:

$$PR(19) = [T_B(19V) - T_B(19H)]/[T_B(19V) + T_B(19H)] \quad (8)$$

$$GR(37V/19V) = [T_B(37V) - T_B(19V)]/[T_B(37V) + T_B(19V)] \quad (9)$$

When PR and GR are plotted against each other, brightness temperature values tend to cluster in two locations, an open water (0% ice) point and a line representing 100% ice concentration, roughly forming a triangle. The concentration of a grid cell with a given GR and PR value is calculated by a linear interpolation between the open water point and the 100% line segment (Figure 5).

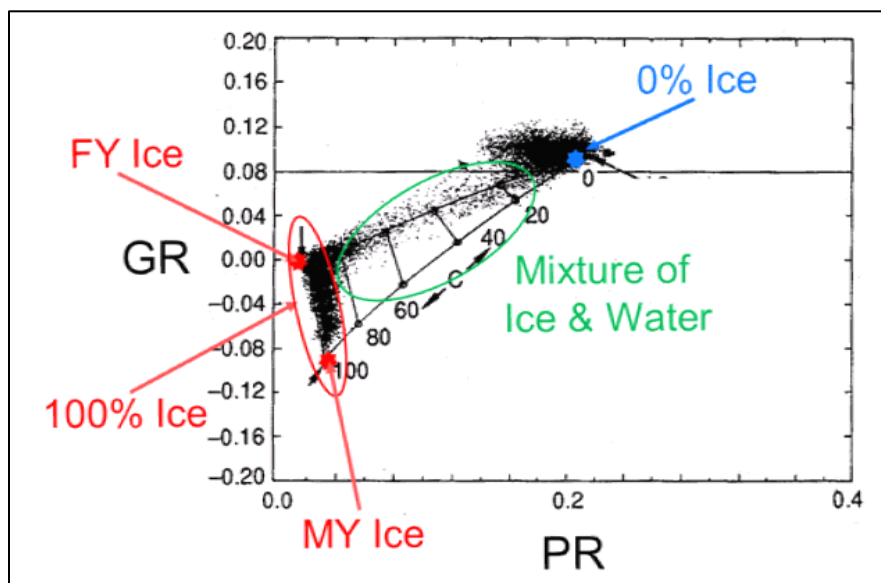


Figure 5: Sample plot of GR vs. PR with typical clustering of grid cell values (small dots) around the 0% ice (open water) point (blue star) and the 100% ice line (circled in red). First year (FY) ice clusters at the top of the 100% ice line, and multi-year (MY) ice clusters at the bottom. Points with a mixture of ice and water (circled in green) fall between these two extremes. Adapted from Figure 10-2 of Steffen et al. (1992).

Mathematically, these two ratios are combined in the following two equations:

$$C_F = (a_0 + a_1PR + a_2GR + a_3PR * GR)/D \quad (10)$$

$$C_M = (b_0 + b_1PR + b_2GR + b_3PR * GR)/D \quad (11)$$

$$\text{where } D = c_0 + c_1PR + c_2GR + c_3PR * GR \quad (12)$$

The C_F and C_M parameters represent ice concentration for two different sea ice types. In the Arctic, these generally correspond to FY ice (C_F : ice that has grown since the previous summer) and MY ice (C_M : ice that has survived at least one melt season). In the Antarctic, due to its small amount of MY ice and different ice characteristics, C_M and C_F do not necessarily correspond to the age types and are simply denoted as Type A and Type B. Total ice concentration (C_T) is the sum of the two partial concentrations.

$$C_T = C_F + C_M \quad (13)$$

The a_i , b_i , c_i ($i=0, 3$) coefficients are empirically derived from nine observed T_{BS} at each of the 3 channels for 3 pure surface types (two sea ice and one open water). These T_{BS} , called tie-points, were originally derived for the SMMR sensor (Cavalieri et al., 1984). The tie-points were adjusted for subsequent sensors via intercalibration of the concentration/extent fields during sensor overlap periods to ensure consistency through the time series (Cavalieri et al., 1999). Tie-point adjustments are made via a linear regression analysis along with additional adjustments for open water tie-points. The tie-point adjustment procedure and tie-point values for all sensors through F13 SSM/I are provided in Cavalieri et al. (1999). Tie-points for F17 are described in Cavalieri et al. (2011). Tie points for AMSR-E and AMSR2 were derived by computing a linear regression between the AMSR versus F17 T_{BS} and applying that relationship to the F17 tie points to derive AMSR tie points. See Table 5.

Note that the NASA Team algorithm can sometimes obtain concentration values that are less than 0% or are greater than 100%, both of which are clearly unphysical. Such values are set to 0% and 100%, respectively.

NIMBUS 7 SMMR				
Arctic		18H	18V	37V
	OW	98.5	168.7	199.4
	FY	225.2	242.2	239.8
	MY	186.8	210.2	180.8
Antarctic				
	OW	98.5	168.7	199.4
	A	232.2	247.1	245.5
	B	205.2	237.0	210.0

DMSP-F8 SSMI				
Arctic		19H	19V	37V
	OW	113.2	183.4	204.0
	FY	235.5	251.5	242.0
	MY	198.5	222.1	184.2
Antarctic				
	OW	117.0	185.3	207.1
	A	242.6	256.6	248.1
	B	215.7	246.9	212.4
DMSP-F11 SSMI				
Arctic		19H	19V	37V
	OW	113.6	185.1	204.8
	FY	235.3	251.4	242.0
	MY	198.3	222.5	185.1
Antarctic				
	OW	115.7	186.2 -0.4	207.1
	A	241.2	255.5	245.6
	B	214.6	246.2	211.3
DMSP-F13 SSMI				
Arctic		19H	19V	37V
	OW	114.4	185.2	205.2
	FY	235.4	251.2	241.1
	MY	198.6	222.4	186.2
Antarctic				
	OW	117.0	186.0	206.9
	A	241.4	256.0	245.6
	B	214.9	246.6	211.1
DMSP-F17 SSMIS				
Arctic		19H	19V	37V
	OW	113.4	184.9	207.1
	FY	232.0	248.4	242.3
	MY	196.0	220.7	188.5
Antarctic				
	OW	113.4	184.9	207.1
	A	237.8	253.1	246.6
	B	211.9	244.0	212.6
AMSR-E/AMSR2				
Arctic		19H	19V	37V
	OW	109.60	190.55	211.20

	FY	234.73	253.07	244.16
	MY	196.75	225.80	193.78
Antarctic				
	OW	110.20	190.79	211.90
	A	242.83	258.78	249.25
	B	215.22	249.71	217.10

Table 5: NASA Team tie-point values (in Kelvin) for each sensor.

3.4.1.2 Bootstrap Algorithm

Like the NASA Team algorithm, the Bootstrap algorithm is empirically derived based on relationships of brightness temperatures at different channels. The current version of the Bootstrap algorithm is 3.1 (Comiso et al., 2017), which is used in the CDR processing. The Bootstrap method uses the fact that scatter plots of different sets of channels show distinct clusters that correspond to pure surface types (100% sea ice or open water) (Comiso, 1986).

Figure 6 shows a schematic of the general relationship between two channels. Points that fall along line segment AD represent 100% ice cover. Points that cluster around point O represent open water (0% ice). Concentration for a point B is determined by a linear interpolation along the distance from O to I where I is the intersection of segment OB and segment AD. This is described by the following equation:

$$C = (T_B - T_O) / (T_I - T_O) \quad (14)$$

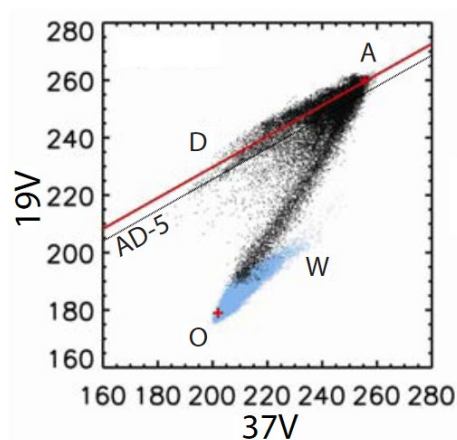


Figure 6: Example of the relationship of the 19V vs. 37V T_B (in Kelvin) used in the Bootstrap algorithm. Brightness temperatures typically cluster around the line segments AD (representing 100% sea ice) and OW (representing 100% open water). For points that fall below the AD-5 line (dotted line), bootstrap uses T_B relationships for 37H vs. 37V. Adapted from Comiso and Nishio (2008).

The Bootstrap algorithm uses two such combinations, 37H versus 37V and 19V versus 37V, denoted as HV37 and V1937, respectively. Points that fall within 5 K of the AD segment in a HV37 plot, corresponding roughly to concentrations > 90%, use this approach. Points that fall below the AD-5 line, use the V1937 relationship to derive the concentration. Slope and offset values for line segment AD were originally derived for each hemisphere for different seasonal conditions (Table 2 in Comiso et al, 1997). However, a newer formulation was developed where slope and offsets are derived for each daily field based on the clustering of sea ice signatures within the daily brightness temperatures (Comiso and Nishio, 2008). This dynamic tie point adjustment allows for day-to-day changes in sea ice microwave characteristics. Further refinements were later done, including adjusting open water tie points (Comiso et al., 2017). It is this latest version of the Bootstrap algorithm (version 3.1), with dynamic sea ice and open water tie points, that is used in version 5 of the CDR.

Intersensor calibration is done similar to the way it is done for the NASA Team algorithm where brightness temperatures from the sensors are regressed against each other. One sensor's brightness temperatures are adjusted based on the regression with the other sensor. However, because the slope and offset values are derived each day based on the brightness temperatures, there are not specific slope/offset (tie-point) adjustments between sensors. Also, while the NASA Team originally derived the tie-points for SMMR and then adjusted future sensors to maintain consistency with SMMR, the newest version of the Bootstrap algorithm used AMSR-E as a baseline and adjusted SSM/I and SMMR brightness temperatures to be consistent with AMSR-E. Because AMSR-E is a newer and more advanced sensor, the intersensor calibration should be more accurate and more consistent overall. This is discussed further in Comiso and Nishio (2008) as well as further minor improvements for the latest version in Comiso et al. (2017).

The algorithm can sometimes obtain concentration values that are less than 0% or are greater than 100%, both of which are clearly unphysical. Such values are set to 0% and 100% respectively.

3.4.1.3 Sea Ice Concentration Climate Data Record Algorithm

NSIDC processes the daily input brightness temperatures into two intermediate sea ice concentrations using the two Goddard-developed algorithms: NASA Team (Cavaliere et al., 1984) and Bootstrap (Comiso, 1986) described above in sections 3.4.1.1 and 3.4.1.2, respectively. Then, these two intermediate sea ice concentrations are merged together using the sea ice concentration CDR algorithm that is described below.

The NASA Team and Bootstrap algorithms are run independently. Then, the algorithm concentration values are combined to create the CDR concentration field by selecting the larger concentration value between the NASA Team and Bootstrap outputs for each grid cell and implementing a 10% concentration threshold based on Bootstrap concentrations. Then, automated QC procedures are applied as described in Section 3.4.1.5. The details and rationale for these steps are provided below:

1. At each sea ice grid cell, the concentration between the NASA Team and the Bootstrap output are compared, and whichever value is greater is selected as the CDR value. Both algorithms tend to underestimate concentration, as is discussed more in Section 5.5, but the source and the effect on the underestimation differs between algorithms. The NASA Team algorithm, because it uses a ratio of brightness temperatures, tends to cancel out any physical temperature effects. The Bootstrap algorithm uses relationships between two brightness temperatures that are dependent on physical temperature. Thus, physical temperature changes can affect Bootstrap estimates. This occurs primarily in regimes with very low temperatures: winter in the high Arctic and near the Antarctic coast (Comiso et al., 1997). During winter conditions with more moderate temperatures, NASA Team concentrations also tend to have a lower bias (Kwok, 2002; Meier, 2005). During melt conditions, both algorithms tend to underestimate concentration; but the effect is more pronounced in the NASA Team algorithm. Similarly, the NASA Team estimates are biased lower than the Bootstrap estimates when melt conditions are present (Comiso et al., 1997; Meier, 2005; Andersen et. al, 2007).

While these characteristics of the algorithm are true in an overall general sense, ice conditions and algorithm performance can vary from grid cell to grid cell; and in some cases, this approach will result in an overestimation of concentration (Meier, 2005). However, using the higher concentration between the two algorithms will tend to reduce the overall underestimation of the CDR estimate.

2. A 10% concentration threshold based on the Bootstrap concentration is used to define the ice edge (the boundary between ice and open water). A 15% cutoff is a common standard that has been in use for many years (Zwally et al., 1983); and in comparison studies with other satellite data, has agreed well, on an average basis, with the observed ice edge (Cavalieri et al., 1991; Meier et al., 2003). Further, the applied weather filters typically remove most concentrations below 15% (Cavalier et al., 1999). However, there are indications that the Bootstrap algorithm can potentially detect ice at as low as 8% levels (Comiso and Nishio, 2008). Thus, a 10% cutoff was chosen for the CDR data fields. However, the validity of this assumption depends on the character of the ice edge as well as ocean and atmospheric conditions and for total extent and area calculations a 15% cutoff is still recommended. The 10% cutoff in the CDR field will miss some real ice, but low concentrations have much higher uncertainties. The 10% cutoff removes many potentially high-error concentration estimates and provides a standard throughout the time series. Because the T_{BS} are gridded using a drop-in-the-bucket method at resolutions that correspond to the center of the observation footprint, the ice edge has a precision of two to three grid cells. Note that because of the temporal interpolation that is applied during post processing, concentrations less than 10 percent can occur in the daily fields.

The monthly average is computed at each grid cell by averaging all available daily values in the month for that grid cell. A minimum of 20 days (10 for SMMR) is required

for a valid monthly value. If a grid cell has fewer than 20 days with non-missing data, that grid cell is assigned the missing flag in the monthly field. No concentration threshold is used in the monthly fields. Monthly concentration values of less than 10% may occur because the average of a grid cell for a month may be lower.

3.4.1.4 Regridding SMMR, SSM/I, and SSMIS

With the release of the version 5 SIC CDR and the addition of the higher resolution AMSR-E and AMSR2 instruments, the nominal grid cell size of the SIC CDR is now 12.5 km x 12.5 km. However, the SMMR, SSM/I, and SSMIS instruments are a lower resolution and have a nominal grid cell size of 25 km x 25 km. To match the lower resolution sensors to the higher resolution ones, a regridding method was applied to up-sample the lower resolution data to the higher resolution. This regridding is done on the sea ice concentration data once it has been processed through the SIC CDR algorithm. There are four cases to consider when performing the regridding operation: 1) SIC grid cells within the pack ice but away from the coast, 2) SIC grid cells at or near the ice edge, 3) SIC grid cells near the coast that have an overlying 25 km grid cell, and 4) SIC grid cells near the coast that do not have an overlying 25 km grid cell. The method to regrid each of these cases is described below:

1. SIC grid cells within the pack ice but away from the coast:

For SIC grid cells that are within the ice pack, that is, grid cells that are further than 3 grid cells away from the ice edge and that are not near the coast, a bilinear interpolation of sea ice concentration values is done to convert a 25 km grid cell into four 12.5 km grid cells.

2. SIC grid cells at or near the ice edge:

For SIC grid cells that are at or near the ice edge, that is, grid cells near the ice edge that are 1, 2, or 3 grid cells away from open ocean, a scaling adjustment is applied to match the lower resolution sensors with the higher resolution sensors. This is done so that the resampled ice edge more closely matches what the ice edge would look like if the native resolution was 12.5 km. Because the lower resolution sensors have larger sensor footprints, the ice edge tends to get “smeared out” (Figure 7). This leads to the delineation of the ice edge outward from the ice pack. The higher resolution sensors can better discriminate the ice edge than the lower resolution sensors (Figure 7). This erosion procedure helps to make the lower resolution data more consistent with the higher resolution.

The procedure to calculate the scaling adjustment is to perform a linear regression between SSMIS and AMSR2 gridded sea ice concentrations at 12.5 km that are orthogonally adjacent to open ocean at 1, 2, and 3 grid cells from the ice edge. The slope of the line that comes out of the linear regression at each distance is used as the scaling factor to reduce the concentration of the lower resolution sensors. The scaling factor used for grid cells 1 grid cell away is 0.70, for grid cells 2 grid cells away is 0.89, and for grid cells 3 grid cells away is 0.97.

Note that we have found that this adjustment may not be aggressive enough because we are still seeing biases between the lower resolution and higher resolution sensors where the lower resolution sensors are seeing more sea ice. We plan to continue to evaluate this adjustment and correct as necessary.

3. **SIC grid cells near the coast that have an overlying 25 km grid cell:**
For SIC grid cells near the coast that have an overlying 25 km grid cell, bilinear interpolation does not always work because, near the coast, there are not always enough surrounding grid cells to do the calculation (green areas in Figure 8). For these grid cells, a nearest-neighbor interpolation is used instead. This means that the value from the 25 km ocean grid cell is used for any of the 4 nested 12.5 km grid cells it overlays.
4. **SIC grid cells near the coast that do not have an overlying 25 km grid cell:**
Because the 12.5 grids are higher resolution, there are grid cells that are marked as ocean in the 12.5 km grid that do not have an overlying ocean pixel in the 25 km grid because the 25 km grid does not resolve the coastline as well (red areas in Figure 8). This means that 12.5 km ocean-cell values need to be extrapolated for these locations. To determine ice concentrations for these cells, a nearest-neighbor interpolation is also used based on the values extrapolated from steps 1, 2, and 3.

NOTE: These adjustments reduce the difference between the resolutions, but they do not necessarily completely remove it, particularly in specific regions or times of year. Users should use caution when investigating trends and variability that span between the SMMR-SSMI-SSMIS period and the AMSR period. Further refinements will be made to reduce this uncertainty.

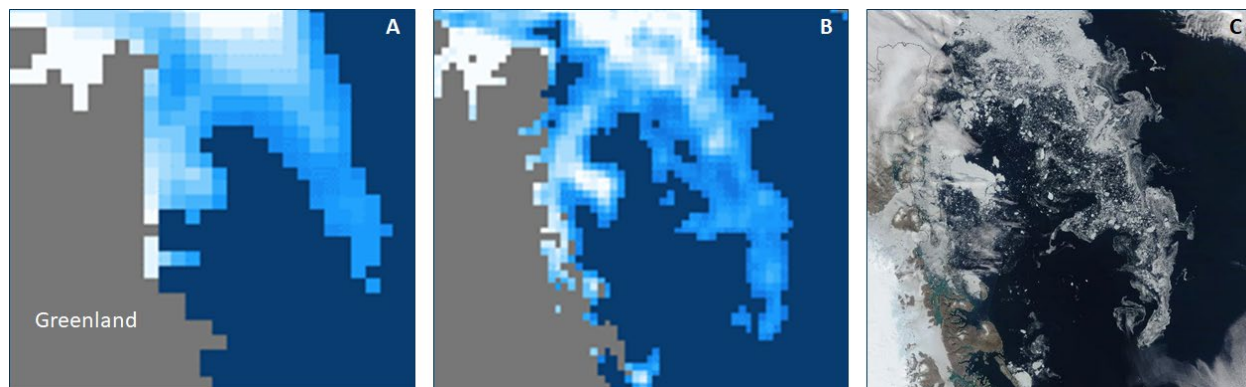


Figure 7. A comparison of sea ice concentration off the NE coast of Greenland for 30 July 2021 for the 25 km SSMIS (A), 12.5 km AMSR2 (B), and 500 m MODIS visible band image (C) sensors. This close-up view shows the better ice edge delineation from AMSR2 over SSMIS to capture features in the ice pack that are visible in the MODIS image. The lower resolution SSMIS image “smears” the ice edge over the larger 25 km x 25 km grid cells.



Figure 8. This image, showing Ellesmere Island and the NW coast of Greenland, highlights the difference of coastal areas between the 12.5 km grids and the 25 km grids. Areas that are ocean in both grids are blue. Areas that are not surrounded by enough ocean pixels for bilinear interpolation to work are green. Areas that are ocean in the 12.5 km grids but are land in the 25 km grids are red. Areas that are land in both grids are black.

3.4.1.5 Quality Control Procedures

Several automated quality control procedures have been implemented to spatially and temporally fill in missing data and to filter out spurious concentration values.

Small amounts of missing data are common in satellite data, especially over a satellite record spanning more than 40 years. Reasons for missing data are numerous and range from issues with the instrument onboard the satellite, satellite viewing angles, and problems arising at the ground stations when data are downloaded from the satellite. These missing data are handled in two ways in the CDR processing code. First, a spatial interpolation is performed on the input brightness temperature data to fill small gaps (a few pixels). Then, temporal interpolation is performed on the sea ice concentration data to fill larger gaps (full swaths or entire days). These are described further in detail in the sections below.

The main sources of the spurious ice grid cells are ocean surface brightness temperature variation, atmospheric emission, and mixed land-ocean IFOV in a grid cell. These are first discussed in general and then the specific filters used to remove much of these effects are described.

Both algorithms assume that open water can be represented as a single point in the clustering of different channel combinations. However, it is evident in Figure 5 and Figure 6 that there is considerable spread around the open water point. This is primarily due to weather effects, namely: roughening of the ocean surface by winds, which

increases the microwave emission of the water; and atmospheric emission, primarily due to water vapor and liquid water (clouds), which will also increase the emission retrieved by the sensor. Atmospheric emission is most pronounced during rain fall over the open ocean. Emission from the atmosphere has the largest effect on the 19 GHz channels because they are near to frequencies in which there is strong water vapor emission.

Spurious ice is also common along ice-free coasts. Because of the large IFOV (up to 72 km x 44 km for the 19 GHz channel on SSMIS), brightness temperature values from ocean grid cells near the coast often contain microwave emission from both land and ocean. These mixed grid cells of ocean/land have a brightness temperature signature that is often interpreted by the algorithms as sea ice. When sea ice is actually present along the coast, the effect is small, but when there is no ice present, artifacts of false ice appear. This is commonly called the land-spillover effect because emission from the land surface “spills over” into ocean grid cells.

Automated filters used to correct these spurious concentrations are discussed further in sections below. It is possible, however, that automated filters may also remove real ice in some conditions.

Brightness Temperature Spatial Interpolation

The input brightness temperatures that are used to produce the sea ice CDR sometimes contain small gaps in the data fields. These occur commonly in the fields, especially in the more equator-ward parts of the grids. This is because of the drop-in-the-bucket (DITB) method used for gridding the brightness temperature swath data. The DITB method simply averages all footprints (swaths) into a grid in a given day based on the center location of the footprint. For example, at each grid cell, all footprints whose centers are within that grid cell’s boundaries are found. However, because the footprints are larger than grid cell size, some grid cells have no footprint centers. Thus, these are empty grid cells (i.e., have a missing or zero value). These happen more equator-ward because there are fewer overlapping swaths and thus more chance of empty grid cells.

These empty grid cells are generally isolated, that is, 1 or 2 missing grid cells surrounded by cells with valid T_B values. To correct for these missing grid cells, they are filled by bilinear interpolation whereby the grid cell is filled with the average of the four grid cells that surround it: one above, one below, one to the left, and one to the right. However, to make the spatial filling algorithm more robust and allow for filling of neighboring missing grid cells, a threshold of at least three out of the four surrounding cells with valid values was set. A flag called `spatial_interpolation_flag` marks the channels that were interpolated. See Section 3.4.3.1 for more information on this flag.

This spatial interpolation is performed on all T_B channels prior to the input data being passed into the sea ice concentration algorithms. Larger gaps in the data are filled by temporal interpolation (see the next section below).

Sea Ice Concentration Temporal Interpolation

To fill larger gaps in the data such as missing swaths or missing days of data, a temporal interpolation is performed on the sea ice concentration data. Once the T_{BS} are processed through the NASA Team, Bootstrap, and CDR sea ice algorithms, the temporal interpolation is applied. The method of interpolation is performed by locating a missing sea ice concentration grid cell on a particular date and then using linear interpolation to fill that value from data on either side of that date. Data can be interpolated with values of up to five days on either side of the missing date and those days do not have to be evenly spaced on either side. For example, a missing grid cell can be interpolated from a data point one day in the past and one day in the future or a data point two days in the past and four days in the future up to a data point five days in the past and five days in the future. This linear interpolation method is the preferred technique of temporal interpolation. However, in some cases, gaps still exist after this interpolation scheme is performed because two data points on either side of the missing value are not found with which to linear interpolate. To attempt to further fill these gaps, a single-sided gap filling is performed whereby we check if there is at least one data value up to three days on either side of the date and then simply copy that value into the missing grid cell. A flag called `temporal_interpolation_flag` marks the data that were interpolated. See Section 3.4.3.1 for more information on this flag.

Pole Hole Spatial Interpolation

A polar orbit and wide swath provide near-complete coverage at least once per day in the polar regions except for a small region around the North Pole called the pole hole. The size of this hole has changed over time as the instruments have become more advanced. See Table 4 for a list of the sizes of the holes by instrument. A spatial interpolation has been applied to the pole hole to fill this area. With the release of the version 5 ECDR, this spatial interpolation has been slightly improved upon. In previous versions, even grid cells around the pole hole that had occasional data were masked out and then an average of the surrounding cells was computed to fill them (red and tan cells in Figure 9). With this version, on a first pass, a temporal interpolation is applied. Data from up to five days prior or following are used to fill pole hole locations with occasional data (red cells in Figure 9). If these are not available, the pole hole is filled with the average of the concentration value from all the grid cells which surround the pole hole (tan cells in Figure 9). All grid cells within the pole hole have the same concentration value. The `spatial_interpolation_flag` variable identifies this region. See Section 3.4.3.1 for more information on this flag.

Note: The current pole hole is quite small (Table 4); and even though the ice edge has retreated a great deal in recent years, the hole is still well within the boundary of where we are confident that ice exists. However, it is important to note that one cannot assume what the concentration is, especially in late Arctic summer and early autumn. Thus, we would advise caution in using the interpolated data in long-term trends or climatology analyses and would generally recommend against it. For time series analysis (trends), users should still apply the pole hole mask (see Section 5.6.1.1). We are filling the hole

to provide a complete field for users that want/need complete fields without gaps (e.g., modelers).

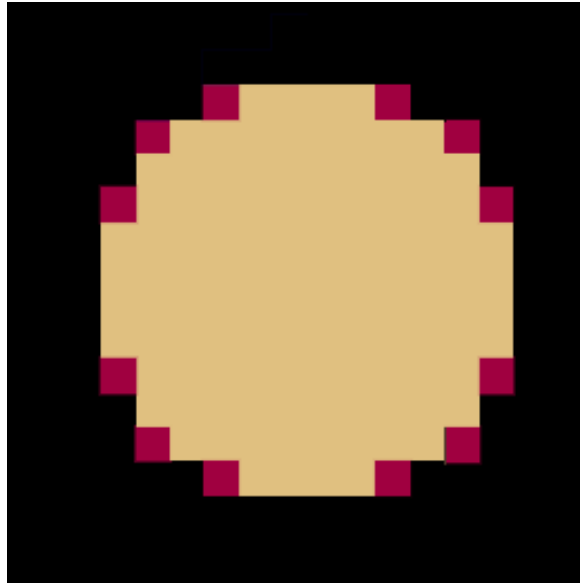


Figure 9. Arctic Pole Hole: Tan grid cells are where there is never any data.
Red cells are where data occasionally occur.

CDR Sea Ice Filtering

Weather effects can cause the passive microwave signature of seawater to appear like that of ice (Cavalieri 1995). Atmospheric water vapor is often the reason behind false-ice detection. Most of these false-ice signatures are removed with a standard brightness-temperature filter, but some are too close to those of real ice and require another method to be removed. Unlike the Goddard products, which apply manual corrections, the CDR uses an automated process to filter any lingering false ice. This is accomplished by applying the NASA Team weather filter and NASA Team 2 land spill over corrections and the Bootstrap weather filter to the CDR sea ice concentrations. This takes the place of the Goddard manual corrections. Although it may not remove all false ice as well as manual correction can, it is a good approximation and is fully traceable. These are described below.

NASA Team Weather Filters

Spurious ice over open water is removed by a threshold of the GR3719 ratio (Equation 9) and an additional GR2219 ratio:

$$GR(22V/19V) = [T_B(22V) - T_B(19V)]/[T_B(22V) + T_B(19V)] \quad (15)$$

Using the following criteria listed in Table 6:

Instrument	Hemisphere	Criteria
SMMR	Northern	GR3719 > 0.070 → concentration = 0 GR2219 → N/A
SMMR	Southern	GR3719 > 0.076 → concentration = 0 GR2219 → N/A
SSM/I	Northern	GR3719 > 0.050 → concentration = 0 GR2219 > 0.045 → concentration = 0
SSM/I	Southern	GR3719 > 0.050 → concentration = 0 GR2219 > 0.045 → concentration = 0
SSMIS	Northern	GR3719 > 0.050 → concentration = 0 GR2219 > 0.045 → concentration = 0
SSMIS	Southern	GR3719 > 0.057 → concentration = 0 GR2219 > 0.045 → concentration = 0
AMSR-E/ AMSR2	Northern	GR3719 > 0.050 → concentration = 0 GR2219 > 0.045 → concentration = 0
AMRR-E/ AMSR2	Southern	GR3719 > 0.057 → concentration = 0 GR2219 > 0.045 → concentration = 0

Table 6. GR3719 and Gr2219 criteria by instrument and hemisphere

Bootstrap Weather Filters

The Bootstrap algorithm also uses combinations of 19V, 22V, and 37V as a weather filter, but the methodology follows the overall Bootstrap by thresholding above a cluster of points in (1) 19V vs. 37V, and (2) 19V vs. (22V-19V) T_B scatter plots (Figure 10).

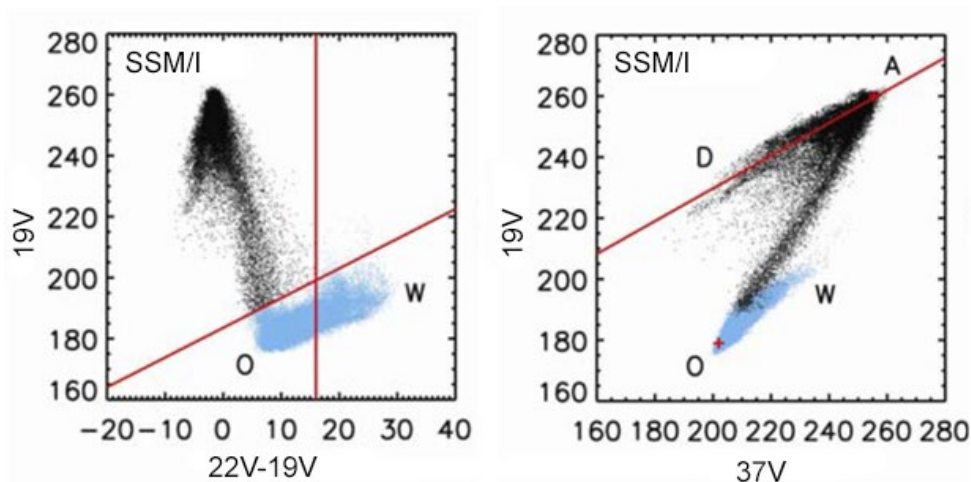


Figure 10: Sample scatter plot of 19V vs. (22V-19V) (left) and 19V vs. 37V (right) T_B s from SSM/I. Values shaded in blue around the OW segment are masked to 0% concentration. From Comiso and Nishio (2008).

NASA Team 2 Land-Spillover Correction

As noted earlier, spurious ice is common along ice-free coasts because the large field of view of passive microwave sensors captures land and ocean together in single grid cells and these signatures get interpreted as sea ice. The NASA Team 2 (NT2) land-spillover correction is a filtering mechanism to automatically remove many of these false coastal ice grid cells. The NT2 land spillover consists of two checks to determine if apparent sea ice is likely to be a misclassification due to nearby land inside the passive microwave sensor's field of view. These are briefly described below. For a full explanation of the NT2 methodology, see Markus and Cavalieri (2009).

1. The algorithm will assume that sea ice along the coast will extend out to at least three grid cells away from land. A land adjacency mask is used to identify these grid cells; it is described in Section 3.3.2. Grid cells that are one or two grid cells from land are considered near-coast and grid cells further away are considered away-from-coast. If a near-coast grid cell does not have any away-from-coast grid cells with at least 50% sea ice concentration within a 7x7 grid cell matrix centered on itself, the near-coast grid cell's concentration is assumed to be false and is set to zero.
2. It is probable that near-coast grid cells will have an apparent sea ice concentration because land appears similar to sea ice at the passive microwave frequencies used in the sea ice concentration calculation. Land pixels are assumed to have an ice concentration of 90%, which is an estimate of the sea ice concentration that the algorithm might be expected to compute simply from the presence of nearby land. A 90% concentration land mask is used in the calculation of this step; it is described in Section 3.3.2. If the calculated sea ice concentration of a near-coast grid cell is less than this value, it is set to zero.

Invalid Ice Masks

As noted in the sections above, false ice can occur from weather effects and land spillover. While weather filters and land-spillover corrections remove much of this false ice, some can remain. Applying an invalid ice mask can help to remove any lingering false ice.

Northern Hemisphere

The best way to evaluate where ice can be is to look at a climatology of sea ice occurrence, where the climatology is built from Arctic-wide sea ice analyses over as long a period as possible from many different sources. These show where ice detected by the satellite data algorithm is most likely to be valid ice, based on where ice has existed in the past.

For the Northern Hemisphere, any remaining weather effects and land spillovers are corrected with the Polar Stereographic Valid Ice Masks Derived from National Ice

Center Monthly Sea Ice Climatologies, available from NSIDC (<https://nsidc.org/data/nsidc-0622>). The climatology used for these masks is the National Ice Center Arctic Sea Ice Charts and Climatologies in Gridded Format. It includes 12 masks showing the maximum sea ice extent, one for each month of the year, over the period 1972 to 2007. In addition, a day-of-year climatology ice mask is applied to the SMMR era only that is derived from the Goddard Bootstrap algorithm NSIDC-0079 data.

Southern Hemisphere

In the Southern Hemisphere, masks based on the monthly sea surface temperature (SST) climatology of Levitus and Boyer (1994) are used to remove remaining false ice. A temperature threshold of 275 K was used to determine the mask boundary for each month. Any sea ice concentrations above 0% calculated by the algorithms in regions where the masks do not allow sea ice are set to zero in the final concentration estimates. In addition, a day-of-year climatology ice mask is applied to the SMMR era only that is derived from the Goddard Bootstrap algorithm NSIDC-0079 data.

3.4.1.6 Comparison of NSIDC-Processed and Goddard-Processed Brightness Temperatures Using the NASA Team and Bootstrap Algorithms

The process that NSIDC uses to convert brightness temperatures to sea ice concentration using the NASA Team and Bootstrap algorithms is very similar to the way Goddard processes their ice concentrations with a few known differences. NSIDC uses a new brightness temperature version for the F8 period from what Goddard used. In addition, NSIDC uses a corrected version of brightness temperatures for F11 and F13, while Goddard used the uncorrected version for their NASA team product but the corrected version for their Bootstrap V3 product. The two processing streams also use different invalid ice masks. Both the NSIDC-processed and Goddard-processed brightness temperatures use a similar automated spatial and temporal interpolation method, however, Goddard also performs an additional manual QC step to remove spurious ice. In comparisons between the two, there are occasional small variances due to the differences noted here. This section describes these differences in more detail.

Goddard processed their sea ice concentrations using the NSIDC gridded brightness temperature version available at the time of processing. For the ECDR, NSIDC is using the data products listed in Table 3.

For F11 and F13, after initial processing of brightness temperatures at NSIDC and NASA Team concentrations at Goddard, small errors were discovered in the brightness temperature processing resulting in the inclusion of some bad scan lines. These bad scan lines resulted in some small artifacts in the gridded Goddard concentration estimates. After discovery of the brightness temperature processing error, NSIDC reprocessed the affected F11 and F13 data. Goddard reprocessed their concentrations

from the Bootstrap algorithm for V3, but the NASA Team concentrations were not reprocessed. However, Goddard performs a manual QC process that removed these bad data.

For missing grid cells, both NSIDC and Goddard employ a spatial and temporal interpolation to fill in the missing values. For isolated missing grid cells, a spatial average from surrounding non-missing brightness temperature grid cells is used to fill the missing grid cell. For larger areas of missing data, due to missing swaths or days of brightness temperature data, a temporal interpolation is used where sea ice concentration estimates from the day before and the day after are averaged to fill the missing region. For this temporal interpolation, Goddard only uses an average of the day before and the day after. If there are still large missing areas, Goddard fills these manually. NSIDC, on the other hand, uses an average of up to five days before and five days after to fill large gaps. Because no manual filling is done for the NSIDC-processed concentrations, this larger time range was utilized to attempt to fill as much missing data as possible. For a complete description of the spatial and temporal interpolation method utilized by NSIDC, see Section 3.4.1.5.

For both NASA team and Bootstrap products, Goddard uses a different Northern Hemisphere invalid ice mask than NSIDC does. Goddard uses the SST-climatology mask (same source as for the SH), while NSIDC uses the NIC chart climatology (nsidc-0622). NSIDC also applies a daily climatology ice mask derived from Bootstrap Sea Ice Concentrations to both hemispheres for the SMMR sensor. Goddard also uses a different land mask than NSIDC does.

The most significant difference between the processing at NSIDC and at Goddard is Goddard's use of a manual inspection to correct grid cells with erroneous concentration values. Each daily field was examined at Goddard and a hand-cleaning process was used to remove any sea ice grid cells that were deemed to be erroneous. The majority of these erroneous sea ice values were false coastal ice that were not removed by the land-spillover correction, and false ice over the ocean that were not removed by either weather filter or the ocean mask. In these cases, the grid cell is simply replaced with a 0% value. In very rare cases, the manual QC deemed some legitimate sea ice grid cells to have clearly incorrect concentration values. These concentration values were removed and the affected grid cells were considered missing. These missing values were then filled by Goddard via the interpolation discussed above. See Section 3.4.1.5 for a description of how the CDR code handles erroneous concentration values.

3.4.2 Data Merging Strategy

Both the NASA Team and Bootstrap algorithms use platform-dependent tie-points to account for changes in sensors and spacecraft. These tie-point adjustments are derived from regressions of brightness temperatures during instrument overlap periods. The adjustments are made at the product level by adjusting the algorithm coefficients so that the derived sea ice fields are as consistent as possible. This approach was found to be more successful than intercalibrating the input brightness temperature fields. There are several

reasons to adopt this approach. First, the products are derived on daily mean gridded brightness temperatures using a simple drop-in-the-bucket average. Each sun-synchronous sensor has a different equatorial crossing time. This means that the gridded brightness temperature for a given grid cell will be comprised of swath brightness temperature values from different times of day from the old sensor versus the new sensor. Because sea ice, as well as the overlying atmosphere, varies over time, this will result in inconsistencies in the brightness temperature signal even when the brightness temperatures themselves are fully intercalibrated. Second, the sea ice varies on scales far smaller than the footprint of the passive microwave sensors. Thus, any retrieved brightness temperature is likely a mixture of several different surfaces (for example, first-year vs. multi-year, smooth vs. rough/ridged, deep snow vs. snow free, etc.). This makes it difficult to directly match up brightness temperatures from different sensors to the same sea ice conditions over which to intercalibrate. Finally, transitions between sensors may result in a change of frequency. Notably, this occurs for SMMR and SSM/I, where the 18.7 GHz channel on SMMR was replaced by a 19.35 GHz channel on SSM/I; and for SSMIS and AMRS-E, where the 19.35 GHz channel on SSMIS was replaced by an 18.7 GHz channel on AMSR-E.

The NASA Team approach uses sensor-specific hemispheric tie-points for each transition (Cavalieri et al., 1999; Cavalieri et al., 2011). The NT tie-points were originally derived for the SMMR sensor and subsequent transitions to SSM/I and SSMIS adjusted the tie-points to be consistent with the original SMMR record. The NT tie-points for AMSR2 were calculated by computing a linear regression from overlapping F17 and AMSR2 brightness temperatures and determining the equivalent TBs for AMSR2 corresponding to the F17 tie-points. The Bootstrap algorithm uses daily varying hemispheric tie-points, derived from analysis of clusters of brightness temperature values in the relevant channels, as in Figure 12 of Comiso (2009), and the adjustment involves a linear regression between brightness temperatures (Comiso and Nishio, 2008).

3.4.3 Algorithm Output

The sea ice CDR code creates daily and monthly NetCDF data files for each hemisphere. Each daily and monthly CDR file contains four primary CDR fields: a CDR concentration estimate, a standard deviation field, a melt onset flag, and a quality assessment field. Each field is on the 12.5 km polar stereographic grid: 608 columns by 896 rows for the Northern Hemisphere (EPSG 3411) and 632 columns by 664 rows for the Southern Hemisphere (EPSG 3412). In the two sub-sections below, the daily and the monthly fields are described in detail.

Note: In addition to the individual daily and monthly NetCDF files, aggregated versions of these files are also produced. For the daily files, there are yearly aggregated files, where a year's worth of daily data is stored in one NetCDF file. For the monthly files, there is one period-of-record file for each hemisphere where all the monthly data are stored in one NetCDF file per hemisphere.

3.4.3.1 Fields in the daily CDR files

The daily files contain the following variables:

1. cdr_seaice_conc
2. crs
3. melt_onset_day_cdr_seaice_conc
4. qa_of_cdr_seaice_conc
5. raw_bt_seaice_conc
6. raw_nt_seaice_conc
7. spatial_interpolation_flag
8. stdev_of_cdr_seaice_conc
9. surface_type_mask
10. temporal_interpolation_flag
11. time
12. x
13. y
14. latitude
15. longitude

These CDR fields are explained below:

1. Sea Ice Concentration CDR

This field, named `cdr_seaice_conc`, contains the sea ice concentration values for the CDR, scaled from 0-100%. See Section 3.4.1.3 for details on how this is calculated.

2. Coordinate Reference System

This field, named `crs`, describes the polar stereographic projection information for these data.

3. Day of Melt Onset

This field, named `melt_onset_day_cdr_seaice_conc`, contains the day of year on which melting sea ice was first detected in each grid cell. Once detected, the value is retained for the rest of the year. For example, if a grid cell started melting on day 73, the value for the grid cell on that day will be 73, as will all subsequent days until the end of the year when it is then reset to the fill value of 255. The melt onset day is only calculated for the melt season: days 60 through 244, inclusive. Before melting is detected or if no melt is ever detected for that grid cell, the value will be 255.

One of the largest contributors to errors in concentration estimates occurs when surface melt begins (see Section 5.5.2). Thus, a melt flag (`melt_start_detected`)

is implemented in the Northern Hemisphere to indicate where melt may be occurring. The melt onset test is performed only in the Northern Hemisphere because the character of the ice cover in the Southern Hemisphere, typified by strong melt-refreeze cycles, does not yield a reliable melt threshold in passive microwave brightness temperature data (Willmes et al., 2009).

The melt flag is a near-real-time version of the Drobot and Anderson (2001) algorithm, which uses a brightness temperature difference threshold to determine whether melt has begun for the overlying snow cover at each sea ice grid cell. The algorithm is implemented as follows:

$$T_B(19H) - T_B(37H) > 2K \rightarrow \text{no melt} \quad (21)$$

$$T_B(19H) - T_B(37H) \leq 2K \rightarrow \text{melt has begun} \quad (22)$$

A long-term melt onset climate dataset, NSIDC-0105, is distributed by NSIDC (<https://nsidc.org/data/nsidc-0105>). That dataset includes a 20-day temporal filter to screen out possible false melt signatures. For simplicity, the temporal filter is not employed in this product. This means that some grid cells flagged as melt may not actually be melting, and thus, the flag is more conservative than the climate dataset. Note that the melt test does not consider any effects of sea ice motion.

The conditions for melt onset at a particular grid cell are the following:

- Melt detected:
 - Concentration \geq 50% at the beginning of the season
 - Grid cell is not land, coast, shore (1 grid cell from coast), near-shore (2 grid cells from coast), or lake
- Current sea ice concentration \geq 50%
- Brightness temperature delta (19H - 37H) $<$ 2K (Drobot and Anderson, 2001)
- Presence of brightness temperatures for both channels (19H, 37H)

Note: To calculate the melt onset for F17 data, the input brightness temperatures are first scaled as follows:

$$19H_{scaled} = 1.021 * 19H - 1.681 \quad (19)$$

$$37H_{scaled} = 1.001 * 37H - 0.650 \quad (20)$$

These equations were derived by a regression between F17 and F13 brightness temperatures during March through September 2007 when there was an overlap period between the two satellites. Regressions were run for each daily average brightness temperature field and slope and intercept values were calculated. These daily slope and intercept values were then averaged over the entire March through September period to derive the equations above. No scaling was needed on the T_{BS} for the AMSR-E or AMSR2 sensors.

The reason for applying this adjustment is to account for differences between the F17 and F13 sensors, including sensor characteristics (sensor footprint, geometry), differences in orbit (time of equatorial crossing), etc. For the NASA Team sea ice concentration algorithm, the differences between the two sensors are accounted for by adjusting the algorithm tie-points (Cavalieri et al., 2011). For the Bootstrap sea ice concentration algorithm, only a regression is needed because tie-points are derived daily from the brightness temperature fields. For the melt onset, Equations 19 and 20 are used to make this adjustment.

4. Quality Assessment (QA) Flags

This field, named `qa_of_cdr_seaice_conc`, provides additional assessment to complement the standard deviation field. This field includes flags for the following conditions: if the BT and NT weather filters were applied, if the NT2 land-spillover correction was applied, if the invalid ice mask was applied, if spatial or temporal interpolation was applied, and the melt state. See Table 7.

The melt state flag can be used in conjunction with the `melt_onset_day_cdr_seaice_conc` variable. The melt state flag simply identifies that melt has been detected but the melt onset variable provides the day of year of the melt onset. The melt state flag is used starting on March 1 (DOY=60), around the time when the maximum sea ice extent is reached each year. Once a grid cell is flagged as melting, it remains so through the rest of the summer until September 1 (DOY=244), roughly the time when extent reaches its minimum value. When the sea ice concentration is zero, the flag will be turned off. In other words, the flag will only be on if melt conditions are met and there is sea ice. Note this is different from the `melt_onset_day_cdr_seaice_conc` variable which, once set, shows the day of melt onset through the rest of the year. Also note that melt may be intermittent initially in the spring (melt, then refreeze, and melt again) and freeze-up begins near the pole well before September 1. Thus, grid cells that are flagged as melt may not actually have melt occurring and the flag should be used only as a guide for the data quality of the CDR concentration estimates and should not be used specifically for studies on melt. Like the `melt_onset_day_cdr_seaice_conc`, the input F17 brightness temperatures are scaled. See the note in number 3, Day of Melt Onset, above for more details.

Table 7 lists the flag values in the QA field, with an explanation for each parameter. Grid cells with more than one flag property contain the sum of both

flags. In general, higher values are more likely to have high errors. Note that 0 is the fill value for this variable.

Condition	Flag Value	Label in NetCDF Variable
BT weather filter applied	1	BT_weather_filter_applied
NT weather filter applied	2	NT_weather_filter_applied
NT2 land spillover correction applied	4	Land_spillover_filter_applied
No T_B input data available	8	No_input_data
Invalid ice mask applied	16	invalid_ice_mask_applied
Spatially interpolation applied	32	spatial_interpolation_applied
Temporal interpolation applied	64	temporal_interpolation_applied
Start of Melt Detected (Arctic only)	128	melt_start_detected

Table 7: List of flag values used in the daily CDR QA field. A grid cell that satisfies more than one criteria will contain the sum of all applicable flag values.

5. NSIDC Bootstrap Sea Ice Concentrations

NSIDC includes the intermediate NSIDC processed Bootstrap sea ice concentration, named `raw_bt_seaice_conc`, in the product suite to provide transparency in the creation of the sea ice CDR product.

These data are similar to the Goddard produced NASA team sea ice concentrations available from NSIDC as the Bootstrap Sea Ice Concentrations from Nimbus-7 SMMR and DMSP SSM/I-SSMIS (<https://nsidc.org/data/nsidc-0079>) except that the weather filters and land-spillover corrections have not been applied.

6. NSIDC NASA Team Sea Ice Concentrations

NSIDC includes the intermediate NSIDC processed daily NASA Team sea ice concentration, named `raw_nt_seaice_conc`, in the product suite to provide transparency in the creation of the sea ice CDR product.

These data are similar to the Goddard produced NASA team sea ice concentrations available from NSIDC as the Sea Ice Concentrations from Nimbus-7 SMMR and DMSP SSM/I-SSMIS Passive Microwave Data (<https://nsidc.org/data/nsidc-0051>) except that the weather filters and land-spillover corrections have not been applied.

7. Spatial Interpolation QC Flag

This field, `spatial_interpolation_flag`, is set for spatially interpolated grid cells. The values are described in Table 8.

Condition	Flag Value	Label in NetCDF Variable
19 GHz vertical brightness temperature spatially interpolated	1	19v_tb_value_interpolated
19 GHz horizontal brightness temperature spatially interpolated	2	19h_tb_value_interpolated
22 GHz vertical brightness temperature spatially interpolated	4	22v_tb_value_interpolated
37 GHz vertical brightness temperature spatially interpolated	8	37v_tb_value_interpolated
37 GHz horizontal brightness temperature spatially interpolated	16	37h_tb_value_interpolated
Pole hole spatially interpolated	32	pole_hole_spatially_interpolated

Table 8. Spatial interpolation flag values. A grid cell that satisfies more than one criteria will contain the sum of all applicable flag values.

8. Standard Deviation of Sea Ice Concentration

This field, named `stdev_of_cdr_seaice_conc`, contains the standard deviation of both the NASA Team and Bootstrap concentration estimate at each ocean/sea ice grid cell for that grid cell and the surrounding 8 grid cells (Table 9). The standard deviation is calculated from the total of two 3 x 3 arrays of grid cells (one of NASA Team concentrations and one of Bootstrap concentrations), for 18 grid cells in total. Land grid cells within the 3 x 3 array are not included in the calculation; thus, along the coast, fewer than 18 values are used. Any missing grid cells (for example, the pole hole in the Northern Hemisphere) are also not included in the standard deviation. A minimum of 6 valid concentration values out of the 18 total are required to compute a standard deviation. Thus, some grid cells within small bays and inlets may not have a standard deviation value; such cells are likely to be potentially affected by land-spillover and should be considered to have high uncertainties.

This field is meant to give an indication of the uncertainties in the daily CDR concentration estimate. It is not a quantitative error estimate and should not be used as such. However, it does provide a useful guide to users as to the relative

accuracy of concentration estimates relative to surrounding grid cells and can be used to derive relative weights for comparisons, interpolations, or assimilation studies. In winter conditions, away from the ice edge or coast where spatial variability occurs, standard deviations are typically a few percent (Cavalieri et al., 1984) and can potentially serve as a quantitative upper limit of the concentration error (Gloersen et al., 1993).

The error sources for sea ice concentration are described in detail below, but high standard-deviation values will generally correspond to regions where concentration errors are likely higher.

First, isolated sea ice grid cells along the coastline that result from the land-spillover issue discussed above will have higher standard deviations compared to ice-free ocean or high concentration ice cover along the coast because of the mixture of ice and open water (0% ice) in the calculation.

Another region of higher errors occurs along the ice-water boundary (the ice edge) due to limitations in the sensor resolution, to motion of the ice during the 24-hour average period, and to melt/growth of ice. These high gradient regions will have high standard deviation values.

Finally, during melt, the surface and atmospheric effects become relatively larger, leading to more spatial variability and higher standard deviation values. The melt also tends to cause the algorithms to underestimate concentration because they incorrectly interpret the surface melt on top of the ice as increased open water. The NASA Team concentrations generally have a large low bias compared to the Bootstrap concentrations. This is the rationale for computing the standard deviation from both of the algorithms instead of the combined CDR estimate or just one of the algorithms. The lower relative bias in the NASA Team during melt compared to Bootstrap will yield increased standard deviation values, better indicating the presence of melt than using only the CDR concentration standard deviation.

Standard deviation values range from 0-1, and the fill value is -1.

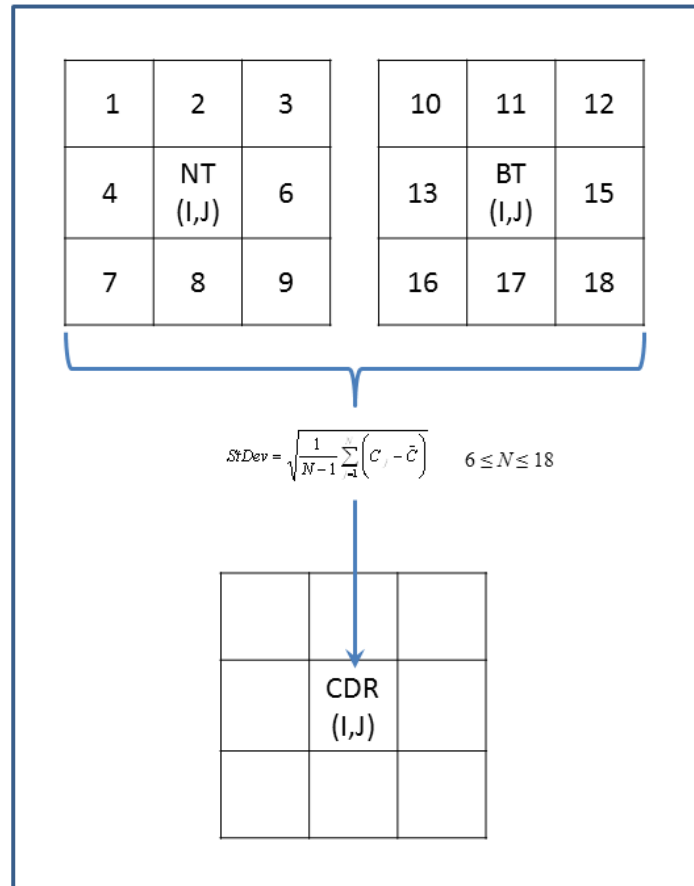


Figure 11: Schematic of grid cell values used in calculation of the CDR standard deviation field. All non-missing ocean/sea ice concentration values (C), from both the NASA Team and Bootstrap algorithm, of the 3 x 3 box surrounding each (I,J) grid cell (up to 18 total values) are used to calculate the standard deviation. A minimum of six grid cells with valid values is used as a threshold for a valid standard deviation.

9. Surface type mask

This field, named `surface_type_mask`, provides a mask of different Earth surface types.

The values are the following:

- 50: ocean
- 75: lake
- 100: polehole_mask (Arctic only)
- 200: coast (land adjacent to ocean)
- 250: land

10. Temporal Interpolation QC Flag

This field, named `temporal_interpolation_flag`, provides details on the grid cells that were temporally interpolated. The value for each flag is a 1- or 2-digit number indicating the pair of known data points used in the interpolation. The first number indicates how many days in the past the data point came from and the second number indicates how many days in the future the data point came from, with a max of 5 days in either direction. For example, if the flag value is 24, then the missing grid cell was interpolated from sea ice concentration data from a grid cell from two days prior and four days in the future. For the linear interpolated values, the smallest flag value is 11 where the missing grid cell was interpolated from a grid cell from one day prior and one day in the future. The largest flag value is 55 where the missing grid cell was interpolated from a grid cell from five days prior and five days in the future. For the secondary interpolation schema, where only one day is used, the lowest value is 1, where the missing grid cell is filled by copying the value from one day in the future. The largest value is 30 where the missing grid cell is filled by copying the value from three days prior.

11. Time

The date of the data (days since 1970-01-01).

12. Xgrid

The projection grid x centers in meters.

13. Ygrid

The projection grid y centers in meters.

14. Latitude

Latitude in degrees north. Note this is found in the aggregated NetCDF files only and not in the individual daily NetCDF files.

15. Longitude

Longitude in degrees east. Note this is found in the aggregated NetCDF files only and not in the individual daily NetCDF files.

3.4.3.2 Fields in the monthly CDR files

The monthly fields are created from all daily files in the given month. The monthly files contain the following variables:

1. cdr_seaice_conc_monthly
2. crs
3. melt_onset_day_cdr_seaice_conc_monthly
4. qa_of_cdr_seaice_conc_monthly
5. stdev_of_cdr_seaice_conc_monthly
6. surface_type_mask
7. time
8. x
9. y
10. latitude
11. longitude

These CDR fields are explained below:

1. Sea Ice Concentration CDR

This field, named `cdr_seaice_conc_monthly`, contains the monthly average sea ice concentration values for the CDR, scaled from 0-100%. See Section 3.4.1.3 for details on how this is calculated.

2. CRS

Describes the polar stereographic projection information for these data.

3. Day of Melt Onset

This field, named `melt_onset_day_cdr_seaice_conc_monthly`, contains the day of year on which melting sea ice was first detected in each grid cell. For the monthly data, this is the value from the last day of the month. Once detected, the value is retained for the rest of the year. For example, if a grid cell started melting on day 73, the variable for the grid cell on that day will be 73, as will all subsequent days until the end of the year. The melt onset day is only calculated for the melt season: days 60 through 244, inclusive. Before melting is detected or if no melt is ever detected for that grid cell, the value will be 255.

4. Quality Assessment Bit Mask

This field, named `qa_of_cdr_seaice_conc_monthly`, contains flags indicating the potential quality of monthly averages. The flags are listed in Table 9. They include whether the average concentration exceeds 15%, which is commonly used to define the ice edge and can be used to easily quantify the total extent.

Another flag indicates when average concentration exceeds 30%, which is a commonly used alternate ice edge definition. It may be desired to remove lower concentration ice that tends to have higher errors. Another flag indicates whether at least half the days have a concentration greater than 15%. This provides a monthly median extent, which may be a better representation of the monthly ice presence because an average conflates the spatial and temporal variation through the month. Additionally, there is a flag that indicates whether at least half the days have a concentration greater than 30%. This also provides a monthly median extent, but this higher percentage may leave out questionable or erroneous ice. There are flags to show if a cell was masked by the invalid ice mask and whether spatial or temporal interpolation was performed. Finally, there is a flag to note whether melt was detected during the month. Since melt tends to bias concentrations lower, this flag gives a sense of whether melt is having a dominating effect.

Condition	Flag Value	Label in NetCDF File
Average concentration exceeds 15%	1	average_concentration_exceeds_0.15
Average concentration exceeds 30%	2	average_concentration_exceeds_0.30
At least half the days have sea ice conc > 15%	4	at_least_half_the_days_have_sea_ice_conc_exceeds_0.15
At least half the days have sea ice conc > 30%	8	at_least_half_the_days_have_sea_ice_conc_exceeds_0.30
Invalid ice mask applied	16	region_masked_by_ocean_climatology
At least one day during month has spatial interpolation	32	at_least_one_day_during_month_has_spatial_interpolation
At least one day during month has temporal interpolation	64	at_least_one_day_during_month_has_temporal_interpolation
Melt detected (at least one day of melt occurred during the month >= 1)	128	at_least_one_day_during_month_has_melt_detected

Table 9: List of flag values used in the monthly CDR QA bit mask. A grid cell that satisfies more than one criteria will contain the sum of all applicable flag values. For example, if spatial interpolation was performed and melt detected then the value will be 160 (32 + 128).

5. Standard Deviation of Concentration

This field, named `stdev_of_cdr_seaice_conc_monthly`, contains the standard deviation (with one degree of freedom) of the daily concentrations in the month. As in the monthly concentration, a minimum of 20 days is required for a valid monthly value. Note that while the daily concentration standard deviation field is based on the variability of the NT and BT concentrations over a 3 x 3 grid cell spatial region, this monthly field is simply the standard deviation of the daily CDR concentrations – i.e., a temporal standard deviation for each grid cell.

6. Surface Type Mask

This field, named `surface_type_mask`, provides a mask of different Earth surface types.

The values are the following:

50: ocean

75: lake

100: polehole_mask (Arctic only)

200: coast (land adjacent to ocean)

250: land

7. Time

The date of the data (days since 1970-01-01).

8. X

The projection grid x centers in meters.

9. Y

The projection grid y centers in meters.

10. Latitude

Latitude in degrees north. Note this is found in the aggregated NetCDF files only and not in the individual monthly NetCDF files.

11. Longitude

Longitude in degrees east. Note this is found in the aggregated NetCDF files only and not in the individual monthly NetCDF files.

4. Test Datasets and Outputs

4.1 Test Input Datasets

The TCDR will be tested against two sea ice concentration data sets at NSIDC: AMSR2 Unified L3 Daily 12.5 km Brightness Temperatures, Sea Ice Concentration, Motion & Snow Depth Polar Grids, Version 1 (https://nsidc.org/data/au_si12/versions/1) and AMSR-E/Aqua Daily L3 12.5 km Brightness Temperature, Sea Ice Concentration, & Snow Depth Polar Grids, Version 3 (https://nsidc.org/data/ae_si12/versions/3).

We worked directly with GSFC investigators and integrated their code into the CDR production. Within the confines of producing a CDR, we have attempted to implement the algorithms and incorporate similar automatic filtering and quality control features to be as consistent as possible with the heritage data products from GSFC while at the same time implementing improvements that produced the most consistent results for the CDR product.

4.2 Test Output Analysis

4.2.1 Reproducibility

The test results can be verified by running the algorithm with the same input T_{BS} and the same ancillary fields and then checking to ensure the results are consistent. For version 3, Peng et al. (2013) and Meier et al. (2014) verified that the CDR algorithm reasonably reproduce the original concentration fields from SSMI and SSMIS provided by NASA Goddard except for the manual corrections and gap-filling interpolations applied by Goddard. In version 4, we have confirmed that the consistency with Goddard extends into the SMMR sensor period, and the added spatial and temporal interpolation address data gaps achieves consistent results with the Goddard products. For version 5, testing against the data sets mentioned in Section 4.1, will confirm the reproducibility.

4.2.2 Precision and Accuracy

The precision and accuracy of the algorithms have been evaluated in numerous studies over the years (for example, Cavalieri et al., 1991; Comiso et al., 1997; Kwok, 2002; Meier, 2005; Andersen et al., 2006, 2007; Ivanova et al., 2014). Overall, the algorithm has a precision of ~5% with an accuracy of ~10%. However, uncertainties are higher under some conditions – most notably near the ice edge and when the surface is undergoing melt. In addition, while filters remove many artifacts (see above), some erroneous ice can still occur over the open ocean due to weather effects and along the coast due to land spillover effects (i.e., mixed ocean and land grid cells).

4.2.3 Error Budget

Much of the error is largely attributable to the limitations of the source data. First, the spatial resolution of the input sensor data for the early part of the time series is limiting. Some input brightness temperature sensor footprints have an effective resolution of ~ 70 km x ~ 45 km. This means that any variability below this resolution (for example, the location of the ice edge) may be missed. The sensor resolution is also the cause of the land spillover issue, where a sensor footprint incorporates a mixture of land and open water, which in some conditions has a signature that is interpreted by the algorithm as sea ice.

With the addition of the Advanced Microwave Scanning Radiometers (AMSR) in version 5 that is a finer resolution sensor, some of these errors have been reduced. However, these records only go back to 2002, so they only improve the record beginning in that year.

Another limitation is surface melt. Passive microwave sensors are sensitive to the phase state of water (liquid or solid), which allows the algorithms to distinguish between sea ice and ocean. However, because microwave emission comes from at or near the surface, water on the surface of the ice is interpreted as liquid. This causes the algorithms to underestimate concentration when ice is melting. The algorithms can be potentially adjusted to reduce this, but then they tend to overestimate concentration during non-melt conditions. Dynamic (automatically varying) daily tie-points alleviate this effect some by allowing the algorithm to adjust to different surface conditions, as is now done within the Bootstrap component of the CDR. See Table 10 for an overview of each of these errors.

Error	Magnitude	Description
Inter-satellite bias	<0.5% of total sea ice extent and area	Inter-calibration has been done to minimize differences in algorithm outputs. Analysis of inter-calibrated retrievals show small differences (Cavalieri et al., 1999; 2012). However, some overlap periods were short and during periods (summer) of high variability. Thus, quantitative values may underestimate the true bias.
Diurnal correction	Undetermined/minimal	Daily average T_B fields are used, which removes most diurnal effects. Different sensors have different orbits that result in some diurnal impacts, but these are implicitly addressed in the satellite intercalibration, which reduces such effects to near zero over most of the ice pack, though larger effects can occur in narrow band near the ice edge. More recent data (since the mid-1990s) have had longer overlaps and thus greater confidence in the consistency between sensors (Meier and Stewart, 2019).
Unknown	Undetermined/	This has not been investigated in detail for the CDR.

calibration drifts	minimal	However, other studies (e.g., Meier and Stewart, 2020) have shown no evidence of significant effects of drift on the sea ice fields.
Effect of changes in surface properties	Undetermined/ minimal	The sea ice algorithms are sensitive to surface conditions and tend to underestimate concentration during melt and for new ice. As melt is occurring earlier and is more widespread, errors in concentration and area trends may result. However, the implementation of dynamic algorithm coefficients (dynamic tie points) within the Bootstrap component of the CDR product can account for seasonal and interannual shifts in surface conditions.

Table 10: Possible error sources and magnitudes for the sea ice CDR

5. Practical Considerations

5.1 Numerical Computation Considerations

No parallelization or difficulties in matrix inversions are expected. Round-off errors exist in conversions between data types (floating point to byte and the reverse), but these are expected and well within the tolerance of the current algorithm and instrument accuracy.

5.2 Programming and Procedural Considerations

The initial daily data can be generated in parallel, along with the temporal interpolation step. Generation of the day of melt parameter is a post processing step and is currently not able to be run in parallel.

The code is implemented in Python and utilizes Conda for managing dependencies on packages like numpy and xarray. Pytest is used for testing. The code base is broken up into three packages: seaice_ecdr, pm_icecon, and pm_tb_data. These are available from GitHub. For a complete set of requirements and environment considerations, see the environment.yml file in each of the packages available at the following GitHub URLs:

- seaice_ecdr: https://github.com/nsidc/seaice_ecdr
- pm_icecon: https://github.com/nsidc/pm_icecon
- pm_tb_data: https://github.com/nsidc/pm_tb_data

5.3 Quality Assessment and Diagnostics

Researchers can assess and improve a CDR by comparing it with operational products. Absolute error can be estimated via comparison to operational sea ice products, such

as those produced by the U.S. National Ice Center (USNIC) or the Canadian Ice Service; but it is important to keep in mind that such products have an operational focus different from the climate focus of the CDR, and the two are not expected to be consistent with each other. Operational ice charts meet the needs of those going into the ice and provide general situational awareness, such as the extent of fast ice or of ice of any concentration greater than zero percent. Chart production is more flexible in order to meet changing user needs and source data availability. USNIC chart products, for example, usually represent sea ice more accurately than do products based on single-sensor satellite data alone. For any given region or day, a user who wants the most accurate analysis of ice edge position and concentration should use products from an operational ice service such as the USNIC. While operational analyses are usually the most accurate and timely representation of sea ice, they have errors and biases that change over time. If one is interested in long-term trends in sea ice or how it responds to changing climate forcing, generally, it is best not to use an operational product, but rather one that is consistently produced and retroactively quality controlled such as this SIC CDR. Section 5.5 describes error assessments between operational products and passive microwave sea ice concentrations.

5.4 Exception Handling

Error cases in the code are caught and informative error messages are printed on exit.

5.5 Algorithm Validation and Error Assessment

Several studies over the years have assessed ice concentration estimates from the NASA Team and Bootstrap algorithms. These assessments have typically used coincident airborne or satellite remote sensing data from optical, thermal, or radar sensors, generally at a higher spatial resolution than the SSM/I and SSMIS instruments but with only local or regional coverage. Several assessments, including ones that use the AMSR sensors, indicate an accuracy of approximately 5% during mid-winter conditions away from the coast and the ice edge (Steffen et al., 1992; Gloersen et al., 1993; Comiso et al., 1997; Meier et al., 2005; Andersen et al., 2007; Belchansky and Douglas, 2002; Meier et al., 2017; Kern et al., 2019). Other assessments suggest concentration estimates are less accurate. Kwok (2002) found that passive microwave overestimates open water by three to five times in winter. Partington et al. (2003) performed a study with the SSM/I instruments and found a difference with operational charts that was relatively low in the winter but rose to more than 20% in summer. A more recent study done by Kern et al. (2020) compared AMSR sensors with MODIS and found similar results.

Errors can come from problems with the sensor, from weather effects, and from inadequacies in the algorithm. For example, a satellite's orbit may drift over time, which may degrade an instrument's data quality. Most SSM/I and SSMIS instruments were in use long past their designed lifetime expectancy. Atmospheric water vapor is a weather effect that can modulate the passive microwave signature of the surface, particularly at

the 19 GHz frequency, causing ice concentration to be overestimated. Finally, while the emissivity of seawater is quite constant, that of sea ice varies considerably depending on many factors including age, thickness, and surface roughness. When one considers that algorithms must arrive at a single number for ice concentration considering the varying brightness temperatures of all the different surface types that may fill the footprints of the 19 GHz and 37 GHz channels and that those footprints differ in size and shape across the instrument swath, one can appreciate the difficulty of the problem. *Microwave Remote Sensing of Sea Ice*, F. Carsey, editor, is a comprehensive overview of the subject (Carsey, 1992). When melt ponds form on the surface of ice floes in the summer, the ice concentration appears to decline when in fact the true concentration may not have changed (Fetterer and Untersteiner, 1998). Melt state is a surface effect that may in itself contain a climate trend, which could influence sea ice concentration trend estimates. This and other concentration error sources have been examined to some extent in Andersen et al. (2007), and their influence appears to be small compared to the estimated sea ice trends, but such effects should be kept in mind when using these data.

5.5.1 Errors from sensor characteristics and gridding scheme

There are four errors that come from the sensor characteristics: (A) sensor noise, (B) the transition between sensors, (C) the large IFOV of the sensors, and (D) the 24-hour composite.

- A. One source of error is simply from sensor noise. The SSM/I and SSMIS sensors have been found to have an RMS error of 0.5 K to 1.0 K (Wentz, 1997). A sensitivity study of NASA Team algorithm concentration found that the concentration sensitivity is about 1-2% per 1 K (Gloersen et al., 1993). Thus, the algorithm precision is about 1%. Overall the error from sensor noise is similar to SSM/I and SSMIS (Imaoka et al., 2010; Ishikawa, 2017).
- B. Another potential sensor error results from the transition between sensors on different satellites. The brightness temperature regression and tie-point adjustment corrects for this, though small artifacts remain (Cavalieri et al., 1999; Comiso and Nishio, 2008). Comparison of ice extent estimates from sensor overlap periods indicate that the adjustments yield agreements that are on the order of 0.05% or less and about 0.5% for sea ice area (Cavalieri et al., 1999; Cavalieri et al., 2011). Short overlap periods of early sensor transitions (SMMR to SSM/I F8 and SSM/I F8 to SSM/I F11) may not account for the full seasonal variability (Meier et al., 2011; Cavalieri et al., 2011) and differences may be higher in some cases. However, differences appear to be well below the sensitivity of the instrument, thus, providing confidence in the robustness of the intercalibrated algorithms through the time series. There is an additional potential error in the transition between the SMMR-SSM/I-SSMIS period and the AMSR period due to change in sensor resolution. Even though the SMMR-SSM/I-SSMIS fields are regridded to match the AMSR resolution and interpolation and

ice edge adjustments are made, inconsistencies may remain, particularly on regional scales.

- C. A more significant limitation of the sensors is the large sensor footprint (IFOV) of the instruments. Though all input brightness temperatures are gridded to the 12.5 km polar stereographic grid, the IFOV of the sensors is coarser than this (Table 2). For the early part of the record, the IFOV of the SSM/I and SSMIS channels are as large as 72 km x 44 km for the 19.35 GHz channel. This means that the sensor is obtaining information from up to a 6 x 4 12.5 km grid cell (75 km x 50 km) region, but that signature is placed into a single grid cell. This results in a spatial “smearing” across several grid cells. For the later part of the record, the IFOV of the AMSR-E and AMSR2 channels are closer to the 12.5 km grid resolution but are still as large as 16 km x 27 km. Further, because a simple drop-in-the-bucket gridding method is used, some grid cells do not coincide with the center of a sensor footprint and, thus, do not have a brightness temperature directly assigned to them even though they are partially covered by at least one footprint. Such grid cells are filled by spatial interpolation (see Section 3.4.1.5 for more information). The coarse resolution also leads to the land-spillover issue of grid cells with a mixture of land and water brightness temperatures that can be interpreted by the algorithms as sea ice.
- D. Another issue is the use of 24-hour composite average brightness temperatures as input for the concentration algorithms. Sea ice can drift with the winds and ocean currents over a 24-hour period, and the surface properties of the sea ice can also change considerably. Thus, the daily brightness temperature fields of the surface properties at a given grid cell are an amalgamation of conditions over 24 hours.

Some of the effect caused by this spatial and temporal compositing of the brightness temperatures is ameliorated because these data have been used consistently for algorithm development, tie-point derivation, intersensor adjustment, and all processing. Thus, these effects, while limiting accuracy on a grid cell level, still yield consistent large-scale trends and variability in the sea ice cover. Regions with sharp gradients in brightness temperature, such as the ice edge and the land/water boundary, are most affected by these characteristics.

Of note is the compositing effect on the precision of the ice edge. First, the ice edge is a region of sharp brightness temperature gradients and rapid (less than 24 hour) variability. Second, there is necessarily ambiguity in the ice edge location due to the limited spatial resolution. For example, an ice edge grid cell (that is, the adjoining grid cells are ice-free) with a 50% concentration could mean that the entire cell has a uniformly distributed 50% ice concentration, that half of the grid is covered by 100% ice and the other half is ice free, or something in between. Because the true spatial resolution is limited by the sensor IFOV and not the grid cell area, even with perfect data and a perfect algorithm, the ice edge can in principle only be discerned to within ~50 km for SMMR, SSM/I, and SSMIS

and ~25 km for AMSR-E and AMSR2. However, the distance between the passive microwave observed (15% concentration) edge and the true ice edge, as determined in ship observations (Ozsoy-Cicek et al., 2009; Ozsoy-Cicek et al., 2011), operational sea ice charts (Partington, 2000), or high resolution satellite data (Meier et al., 2003; Meier, 2005), may be much larger than that.

5.5.2 Errors due to surface variation and ambiguities

There are four primary error sources from surface variation and ambiguities: (A) ice type, (B) ice surface variation, (C) physical temperature, and (D) surface melt.

- A. While five passive microwave channels are potentially available for discriminating sea ice, not all are completely independent and in practice only three surface types are retrievable, one water and two ice (multi-year and first-year). However, two ice types cannot fully describe the complex surface of the sea ice. Tie-points are derived based on “pure surface types” of 100% ice, typically for thick multi-year or first-year ice (for the Arctic). The actual emission from thin ice (as indicated by the brightness temperature) varies with ice thickness up to perhaps 30 cm. Thus, thin ice cover appears in the algorithms as a mixture of water and thick ice. So, thin ice concentration is often underestimated. Algorithms using specific thin ice tie-points have been developed (Cavalieri et al., 1994), but these are not applicable for hemispheric datasets. Because ice quickly grows thicker in winter months, thin ice tends to constitute a small fraction of the overall ice cover, but can result in large error near the ice edge and regions dominated by thin ice (such as the Sea of Okhotsk). Validation studies indicate that the Bootstrap algorithm is more sensitive to thin ice, and thus, more accurate in those regions than the NASA Team algorithm (Partington, 2000).
- B. Beyond thin ice, other sea ice surface variability factors impact the brightness temperature signal, including snow cover, frost flowers, and variations in ice salinity. During winter conditions, these effects are generally small, resulting in average concentration errors of a few percent (Gloersen et al., 1993), though higher errors can occur and are most often underestimations. For example, a comparison between passive microwave sea ice concentrations and concentration derived from high-resolution SAR scenes found that SAR showed less than 0.5% open water area in winter mid-pack sea ice while Bootstrap and NASA Team estimates had 1-3% open water.

Algorithms have been developed to also employ the higher frequency channels (85.5 GHz on SSM/I) to provide additional information (Markus and Cavalieri, 2000; Spreen et al., 2008). However, these algorithms typically require ancillary atmospheric data and/or radiative transfer modeling because the high frequency channels are more sensitive to atmospheric emission. Also, the high frequency data have anomalies in the early part of the time series, limiting the length of the record, and unlike the lower frequency channels, are not available at all for the 1978-1987 SMMR record.

- C. Physical temperature can also cause errors in the sea ice retrieval. Brightness temperature is a function of both the surface emissivity and the physical temperature. So, changes in physical temperature change the retrieved brightness temperature and hence the concentration. The algorithm tie-points implicitly account for a physical temperature, but large variations in temperature can cause errors. The Bootstrap algorithm concentrations have a low bias in extremely cold conditions, typically during the mid-winter season in the high Arctic and near the Antarctic coast. Use of daily tie-points limits this effect, but estimates are still biased low. The NASA Team algorithm uses brightness temperature ratios, so the effect of physical temperature largely cancels out within the algorithm equations.
- D. The largest surface effect on the retrieved concentration accuracy is surface melt. When the snow cover overlying the sea ice begins to melt, the microwave emission changes significantly because of the different emissive properties of water in the frozen state versus the liquid state (Eppler et al., 1992). The brightness temperature values over melting snow and ice are effectively interpreted by the algorithms as a mixture of sea ice and open water. The effect is further exacerbated when melt ponds form on the surface of the ice. Thus, a substantial low bias in summer concentrations of 20-30% from both NASA Team and Bootstrap algorithms has been found in numerous studies (Agnew and Howell, 2003; Gloersen et al., 1993; Cavalieri, 1994; Comiso et al., 1997; Partington, 2000; Meier, 2005)

5.5.3 Errors due to atmospheric effects

A significant advantage of passive microwave data for sea ice concentration retrieval is that atmospheric emission is typically in the frequencies used in the algorithms. This provides all-sky capabilities and allows satellite passive microwave sensors to obtain complete, daily sea ice concentration fields no matter the weather or the season.

However, while atmospheric emission or atmosphere-induced surface emission is typically small, it can cause significant errors in some situations. The atmosphere primarily affects the algorithms over open water and thin ice.

The first effect is not direct emission by the atmosphere but an induced effect. Wind blowing over the ocean roughens the surface, which increases the emission. Even a relatively light wind (for example, 5 m/s) can increase emission enough to register several percent concentration of sea ice when no ice is present (Gloersen et al., 1993; Andersen et al., 2006). The use of weather filters and a 15% concentration threshold eliminates most, but not all, wind effects.

The primary atmospheric emission sources are water vapor and liquid water in clouds. These sources also increase the emission retrieved by the sensor and serve to erroneously increase ice concentration. Sensitivity studies for SSM/I and SSMIS indicate that these effects can be up to a 10-20% concentration bias for open water,

with decreasing effects as sea ice concentration increases (Maslanik, 1992; Oelke, 1997; Andersen et al., 2006). Thus, such effects are primarily limited to open water and near-edge sea ice grid cells. The weather filters and the 15% threshold remove much of the effect over water, but some artifacts may remain. Although the authors are unaware of similar studies for AMSR-E and AMSR2, the effects are likely similar.

5.5.4 Summary of error sources and magnitudes

Table 11 summarizes the error sources, expected potential magnitude of the error, the spatial and/or temporal regime, and the relative effect on each algorithm (BT, NT). These are ranges of typical values as reported in the cited validation studies. Errors at any given grid cell may be larger. Note that many errors will be mitigated in the monthly average fields. Thus, monthly averages are generally more accurate and more stable and are better suited for climate analyses.

Error Source	Typical Magnitude and bias (if any)	Spatial/Temporal Regime	Relative Effect on Algorithm
Sensor Noise	+/-1%	All	NT and BT
Ifov/Gridding	<5%	Winter, pack ice	NT and BT
Ifov/ Gridding	0-100%	Sharp gradients (e.g., ice edge, coast)	NT and BT
Intersensor calibration	~0.1%	All	NT and BT
Physical temperature	<5%, low	Winter, cold	BT more than NT
Non-melt surface variation	<5%, low	Winter, central pack ice	NT more than BT
Thin ice	~30-50%, low	Near ice edge, fall freeze-up	NT more than BT
Surface melt	~10-30%, low	Summer	NT more than BT
Wind	5-20%, high	Open water	NT and BT
Water Vapor, Liquid Water	0-20%, high	Open water and ice near edge	NT and BT

Table 11: List of error sources and typical error magnitudes in % concentration for the NASA Team (NT) and Bootstrap (BT) algorithms with biases and typical regimes.

5.6 Processing Environment and Resources

Data were processed on virtual machines provisioned with all of the code's dependencies using NSIDC infrastructure. Once this code package has been operationalized, more details will be provided in this section about environment and resources needed to run the code.

5.6.1 Look-Up Table Description

Within the code package, there are static ancillary data grids and masks used to create this product. These grids and masks have been organized into the following ancillary files: ecdr-ancillary-psn12.5.nc, ecdr-ancillary-psn25.nc, ecdr-ancillary-psn25.nc, ecdr-ancillary-psn25.nc, ecdr-ancillary-psn25-smmr-invalid-ice.nc, and ecdr-ancillary-pss25-smmr-invalid-ice.nc. This section describes these ancillary files. For an in-depth description of the purpose of the ancillary data, see Section 3.3.2.

5.6.1.1 ECDR Ancillary Files

There are four of these files: ecdr-ancillary-psn12.5.nc, ecdr-ancillary-psn25.nc, ecdr-ancillary-psn25.nc, ecdr-ancillary-psn25.nc. There are two for the 12.5 km grids, one for each of the hemispheres; and two for the 25 km grids, one for each of the hemispheres. These NetCDF files contain the masks and grids in variables within the NetCDF file. These are described in Table 13.

Mask/Grid	Description
adj123	Land adjacency mask that describes how far an ocean pixel is from land. The options are 1 grid cell from land, 2 grid cells from land, 3 grid cells from land, or not near land (>3 grid cells).
crs	Coordinate reference system description of the polar stereographic projection.
invalid_ice_mask	An invalid ice mask that denotes areas of the grid that should not contain sea ice based on climatological analyses of seasonal sea ice locations. There are 12 masks (one for each month). This variable is used in combination with the month variable to differentiate the different monthly masks.
l90c	A mask that defines the coast (land adjacent to water) as 90% sea ice concentration. This mask is needed in the calculation of the NT2 land spillover correction.
latitude	Latitude of each grid cell in degrees north.
longitude	Longitude of each grid cell in degrees east.
min_concentration	A minimum concentration matrix that is used for a land spillover correction. Not currently used in the calculation of the ECDR.
month	The 12 months of the year. Used in combination with the invalid_ice_mask variable to differentiate the different monthly masks.
polehole_bitmask	This is a bitmask that denotes the different pole holes for each satellite/sensor used in the creation of the ECDR. This is used for masking out the northern hemisphere pole hole (an area of the earth that is not measured by the sensor due to the earth incidence angle). Because this is a bitmask, the values are additive. For example, the AMSR2 pole hole is the smallest of the pole holes so it fits inside the others. Therefore, it's value is 127 which is the sum of all the bitmask

	<p>values. The values for each bit are the following:</p> <p>1: Nimbus 7 SMMR pole hole</p> <p>2: DMSP F08 SSM/I pole hole</p> <p>4: DMSP F11 SSM/I pole hole</p> <p>8: DMSP F13 SSM/I pole hole</p> <p>16: DMSP F17 SSMIS pole hole</p> <p>32: Aqua AMSR-E pole hole</p> <p>64: GCOM-W1 AMSR2 pole hole</p>
surface_type	<p>This is a land surface type mask. It defines the following surface types:</p> <p>50: ocean</p> <p>75: lake</p> <p>200: coast (land adjacent to ocean)</p> <p>250: land</p>
x	The x coordinate of the projection.
y	The y coordinate of the projection.

Table 12. ECDR Ancillary Files Content Description

The files reside here:

```
v05r00_ancillary/
  ecdr-ancillary-psn12.5.nc
  ecdr-ancillary-psn25.nc
  ecdr-ancillary-psn25.nc
  ecdr-ancillary-psn25.nc
```

5.6.1.2 SMMR Daily Climatology Invalid Ice Masks

There are two of these files: ecdr-ancillary-psn25-smmr-invalid-ice.nc and ecdr-ancillary-pss25-smmr-invalid-ice.nc. These are day-of-year climatology invalid ice masks derived from the Goddard Bootstrap algorithm NSIDC-0079 data. These are needed for the older SMMR era data to remove weather effects because the 22 GHz channel that is used for weather filtering for the other sensors is not accessible for SMMR.

```
v05r00_ancillary/
  ecdr-ancillary-psn25-smmr-invalid-ice.nc
  ecdr-ancillary-pss25-smmr-invalid-ice.nc
```

6. Assumptions and Limitations

As noted elsewhere, a primary limitation is the spatial resolution (sensor footprint) of the input data, which limits the detail that can be retrieved by the algorithm. The product is on a 12.5 km (nominal) resolution grid, the precision of the ice edge location is limited to ~12.5 km at best. Also, the resolution of the input data varies by sensor and thus some

input data has a resolution as large as ~70 km x ~45 km. This means that small-scale features are not explicitly resolved by the algorithm. This is generally not sufficient for operational support (for example, navigational guidance) and the product should not be used for such purposes. The primary application of the product is for long-term climate monitoring and general guidance on overall regional and global sea ice concentrations, not operational and/or local applications.

The merging of the lower resolution SMMR-SSMI-SSMIS fields with the higher resolution AMSR-E and AMSR2 fields. As noted above, a method has been implemented to match extent based on spatial erosion of SMMR-SSMI-SSMIS. However, this method is basic and has had limited validation. Users should apply caution in investigating trends and variability between the SSMI-SSMIS and AMSR-E/AMSR2 periods.

6.1 Algorithm Performance

The algorithm is empirically derived based on the microwave emission of pure surface types. Because of the number of sensor frequency and polarization combinations that are completely independent, only three surface types can be discriminated by the algorithm – two for sea ice and one for open water. However, the sea ice surface is highly heterogeneous. The microwave signature of ice varies based on ice thickness (up to ~50 cm), snow cover, and melt state. For a global, long-term algorithm, the algorithm is tuned to thick, cold sea ice conditions. This means that the algorithm tends to underperform in regions of thin ice and during melt conditions. Heavy snow cover can also impact the algorithm retrieval, especially if the snow grain size changes significantly and/or there are melt/re-freeze events. Over open water, ocean waves and/or atmospheric emission (especially by liquid water clouds) can increase the surface emission signal and result in false ice retrieval. Weather filters (discussed previously in Section 3.4.1.5) have been included to ameliorate as much of these effects as possible, but occasionally some false ice can still occur.

6.2 Sensor Performance

The sensor performance is dependent on the operation teams that monitor them. Radiometric calibration between sensor transitions is corrected by the sensor-specific tie-point adjustments used by the algorithm, but changes in calibration within a sensor are not addressed. The concentration fields are monitored and sudden changes are an indication of changes in calibration or some other sensor malfunction. Generally, these spurious changes have been short-lived, but when they are chronic, the algorithm can be transitioned to use a new sensor. Radiometric noise for the passive microwave sensors has not been an issue.

7. Future Enhancements

Other enhancements in the sea ice concentration CDR will be considered for the future, pending available funding. Some of the main potential enhancements are discussed below.

7.1.1 Improved Resolution Matching Between SMMR-SSM/I-SSMIS and AMSR-E/AMSR2

The current method of eroding the ice edge of the SMMR-SSM/I-SSMIS fields to match AMSR-E and AMSR2 is a basic approach. While it appears to generally work reasonably well on a large-scale, there are refinements that can be made for greater consistency. The authors plan to investigate more sophisticated methods that may perform better.

7.1.2 Reprocessing Using a New Version of Brightness Temperatures

The current CDR product is based on multiple versions of RSS brightness temperatures for SSM/I, SSMIS, and AMSR-E, and JAXA brightness temperatures for AMSR2. The intersensor adjustments between F13 and F17 were made using these versions of brightness temperatures, so any differences in RSS versions should be accounted for within the algorithm intersensor adjustments. However, the authors aim to do a full reprocessing with a consistent, updated brightness temperature product. The NASA Global Precipitation Mission (GPM) Level 1C (L1C) dataset provides fully intercalibration brightness temperatures for all SSMI and SSMIS instruments as well as AMSR-E and AMSR2 (https://pps.gsfc.nasa.gov/Documents/L1C_ATBD_v1.9_GPMV07.pdf). We will investigate these products for a potential full reprocessing of the sea ice product when resources allow.

7.1.3 EASE-Grid 2.0 Version of Sea Ice CDR

The NASA MEaSUREs enhanced EASE-Grid 2.0 (EASE2) gridded product (<https://nsidc.org/data/nsidc-0630>) uses swath brightness temperatures based on the L1C processing and is currently being updated to use the latest L1C. This MEaSUREs product uses the L1C T_B swath data to create twice-daily T_B composites on the EASE2 grid, including enhanced resolution fields. These T_B s are now being routinely processed by the NASA DAAC at NSIDC and ongoing production, including near-real-time fields, is being supported by the DAAC. These would provide a suitable source of already-gridded fields. The EASE2 grid is equal area, which is easier to work with, and it includes standard geographic parameters (ellipsoid, datum, etc.) that make the data more compatible with modern software packages such as Python and GIS.

7.1.4 New Algorithm Coefficients for Calibration

While intercalibration has been done on the current input data and algorithm coefficients (tie points) are varying (by satellite for NASA Team, daily for Bootstrap), further enhancement is possible and may be necessary for transition to new brightness temperatures. The approach would follow the Bootstrap methodology to continue to allow daily-varying tie points, with adaptations to the NASA Team, and potential further refinements.

7.1.5 Improved Pole-Hole Filling

The current pole-hole fill is a simple average, based on the average concentration of surrounding cells. This provides a reasonable gap-fill but does not include any spatial variability. We will investigate new methods to add realistic spatial variability to the pole hole.

7.1.6 Fill Remaining Temporal Gaps Using Statistical Modeling

While the temporal and spatial interpolation fills most gaps, there are still some periods that do not have data, most notably, Dec 1987 and Jan 1988. This is a large time gap where simple temporal interpolation is not reasonable. However, more advanced methods are possible, including statistical modeling approaches. We will investigate such methods to fill that 1987-1988 and other smaller remaining gaps. Because the gap is so larger and the method will be unique, we may decide to provide this as an ancillary product so that users more clearly understand that that period is missing data and the “data” during that period is based on statistical modeling.

8. References

Agnew, T., and S. Howell (2003). The use of operational ice charts for evaluating passive microwave ice concentration data. *Atmos. Ocean*, 41(4): 317-331.

Andersen, S., R. Tonboe, S. Kern, and H. Schyberg (2006). Improved retrieval of sea ice total concentration from spaceborne passive microwave observations using numerical weather prediction model fields: An intercomparison of nine algorithms. *Rem. Sens. Env.*, 104: 374-392.

Andersen, S., R. Tonboe, L. Kaleschke, G. Heygster, and L.T. Pedersen (2007). Intercomparison of passive microwave sea ice concentration retrievals over the high-concentration Arctic sea ice. *J. Geophys. Res.*, 112, C08004, doi:10.1029/2006JC003543.

- Belchansky, G.I., and D.C. Douglas (2002). Seasonal comparisons of sea ice concentration estimates derived from SSM/I, OKEAN, and RADARSAT data. *Rem. Sens. Environ.*, 81: 67-81.
- Brodzik, M. J., D. G. Long, M. A. Hardman, A. Paget, and R. Armstrong. 2016, Updated 2020. MEASUREs Calibrated Enhanced-Resolution Passive Microwave Daily EASE-Grid 2.0 Brightness Temperature ESDR, Version 1. [Boulder, Colorado USA. NASA National Snow and Ice Data Center Distributed Active Archive Center. doi: <https://doi.org/10.5067/MEASURES/CRYOSPHERE/NSIDC-0630.001>.
- Cavalieri, D.J., P. Gloersen, and W.J. Campbell (1984). Determination of sea ice parameters with the NIMBUS-7 SMMR. *J. Geophys. Res.*, 89(D4): 5355-5369.
- Cavalieri, D. J., J. P. Crawford, M. R. Drinkwater, D. T. Eppler, L. D. Farmer, R. R. Jentz, and C. C. Wackerman (1991). Aircraft Active and Passive Microwave Validation of Sea Ice Concentration From the Defense Meteorological Satellite Program Special Sensor Microwave Imager. *J. Geophys. Res.*, 96(C12): 21989–22008.
- Cavalieri, D. (1994). A microwave technique for mapping thin sea-ice. *J. Geophys. Res.*, 99(C6), 12561-12572.
- Cavalieri, D., C. Parkinson, P. Gloersen, J. Comiso, and H. J. Zwally (1999). Deriving Long-term Time Series of Sea Ice Cover from Satellite Passive-microwave Multisensor Data Sets. *J. of Geophys. Res.*, 104(C7):15,803-15,814.
- Cavalieri, D., C. Parkinson, N. DiGirolamo, A. Ivanov (2011). Intersensor calibration between F13 SSM/I and F17 SSMIS for global sea ice data records. *IEEE Geosci. Remote Sens. Lett.*, 9(2), 233-236, doi:10.1109/LGRS.2011.2166754.
- Cho, K., N. Sasaki, H. Shimoda, T. Sakata, and F. Nishio (1996). Evaluation and Improvement of SSM/I Sea Ice Concentration Algorithms for the Sea of Okhotsk. *J. Rem. Sens. of Japan*, 16(2):47-58.
- Comiso, J.C. (1986). Characteristics of arctic winter sea ice from satellite multispectral microwave observations. *J. Geophys. Res.*, 91(C1): 975-994.
- Comiso, J. C., D. Cavalieri, C. Parkinson, and P. Gloersen (1997). Passive Microwave Algorithms for Sea Ice Concentrations: A Comparison of Two Techniques. *Rem. Sens. of the Environ.*, 60(3):357-384.
- Comiso, J. C., and F. Nishio (2008). Trends in the Sea Ice Cover Using Enhanced and Compatible AMSR-E, SSM/I, and SMMR Data. *J. of Geophys. Res.*, 113, C02S07, doi:10.1029/2007JC0043257.
- Comiso, J. C. (2009). Enhanced Sea Ice Concentrations and Ice Extents from AMSR-E Data. *J. Rem. Sens. of Japan*, 29(1):199-215.

- Comiso, J.C., R.A. Gersten, L.V. Stock, J. Turner, G.J. Perez, and K. Cho. 2017. Positive Trend in the Antarctic Sea Ice Cover and Associated Changes in Surface Temperature. *J. Climate*, 30, 2251–2267, <https://doi.org/10.1175/JCLI-D-16-0408.1>
- Drobot, S. and M. Anderson (2001). Comparison of Interannual Snowmelt Onset Dates with Atmospheric Conditions. *Annals of Glaciology* 33: 79-84.
- Eppler, D.T., and 14 others (1992). Passive microwave signatures of sea ice, in "Microwave Remote Sensing of Sea Ice." F.D. Carsey, ed., *American Geophysical Union Monograph* 68, Washington, DC:47-71.
- Gloersen, P. and F. T. Barath. 1977. A Scanning Multichannel Microwave Radiometer for Nimbus-G and SeaSat-A. *IEEE Journal of Oceanic Engineering* 2:172-178.
- Gloersen, P and L. Hardis. 1978. The Scanning Multichannel Microwave Radiometer (SMR) experiment. *The Nimbus 7 Users' Guide*. C. R. Madrid, editor. National Aeronautics and Space Administration. Goddard Space Flight Center, Maryland.
- Gloersen, P., W.J. Campbell, D.J. Cavalieri, J.C. Comiso, C.L. Parkinson, and H.J. Zwally (1993). Arctic and Antarctic sea ice, 1978-1987: Satellite passive-microwave observations and analysis. *NASA Spec. Publ.* 511, 290 pp.
- Hallikainen, M., and D.P. Winebrenner (1992). The physical basis for sea ice remote sensing, in "Microwave Remote Sensing of Sea Ice", F.D. Carsey, ed., *American Geophysical Union Monograph* 68, Washington, DC:29-46.
- Imaoka, K., Kachi, M., Kasahara, M., Ito, N., Nakagawa, K., & Oki, T. (2010). Instrument performance and calibration of AMSR-E and AMSR2. *International archives of the photogrammetry, remote sensing and spatial information science*, 38(8), 13-18.
- Ishikawa, T., Noguchi, T., Yokobori, S., Ito, T., Taniguchi, M., Okada, Y., & Kasahara, M. (2017). On-orbit performance of High Temperature Noise Source (HTS) for advanced microwave scanning radiometer 2 (AMSR2) onboard the GCOM-W satellite. In *2017 IEEE International Geoscience and Remote Sensing Symposium (IGARSS)* (pp. 522-525). IEEE.
- Ivanova, N., O.M. Johannessen, L.T. Pedersen, and R.T. Tonboe (2014). Retrieval of Arctic sea ice parameters by satellite passive microwave sensors: A comparison of eleven sea ice concentration algorithms, *IEEE Trans. Geosci. Remote Sens.*, 52(11), 7233-7246, doi:10.1109/TGRS.2014.2310136.
- J. P. Hollinger, J. L. Peirce and G. A. Poe. (1990). "SSM/I instrument evaluation," in *IEEE Transactions on Geoscience and Remote Sensing*, vol. 28, no. 5, pp. 781-790. doi: 10.1109/36.58964.

- Kern, S., Lavergne, T., Notz, D., Pedersen, L. T., & Tonboe, R. (2020). Satellite passive microwave sea-ice concentration data set inter-comparison for Arctic summer conditions. *The Cryosphere*, 14(7), 2469-2493.
- Kern, S., Lavergne, T., Notz, D., Pedersen, L. T., Tonboe, R. T., Saldo, R., & Sørensen, A. M. (2019). Satellite passive microwave sea-ice concentration data set intercomparison: closed ice and ship-based observations. *The Cryosphere*, 13(12), 3261-3307.
- T. Kawanishi *et al.* (2003). The Advanced Microwave Scanning Radiometer for the Earth Observing System (AMSR-E), NASDA's contribution to the EOS for global energy and water cycle studies. *IEEE Transactions on Geoscience and Remote Sensing*, 41(2), 184-194. doi: 10.1109/TGRS.2002.808331.
- Kunkee, D.B., G.A. Poe, D.J. Boucher, S.D. Swadley, Y. Hong, J.E. Wessel, and E.A. Uliana (2008). Design and evaluation of the first Special Sensor Microwave Imager/Sounder. *IEEE Trans. Geosci. Remote Sens.*, 46(4), 863-883.
- Kwok, R. (2002). Sea ice concentration estimates from satellite passive microwave radiometry and openings from SAR ice motion. *Geophys. Res. Lett.*, 29(9), 1311, doi:10.1029/2002GL014787.
- Levitus, S. and Boyer, T.P (1994). World Ocean Atlas 1994, Volume 4: Temperature, NOAA National Oceanographic Data Center, Ocean Climate Laboratory, U.S. Department of Commerce, Washington D.C.
- Markus, T. and D.J. Cavalieri (2009). The AMSR-E NT2 Sea Ice Concentration Algorithm: its Basis and Implementation. *Journal of the Remote Sensing Society of Japan*, 29(1): 216-225.
- Markus, T., and D.J. Cavalieri (2000). An enhancement of the NASA Team sea ice algorithm. *IEEE Trans. Geosci. Remote Sens.*, 38(3): 1387-1398.
- Markus, T., J.C. Stroeve, and J. Miller (2009). Recent changes in Arctic sea ice melt onset, freezeup, and melt season length, *J. Geophys. Res.*, 114, C12024, doi:10.1029/2009JC005436.
- Maslanik, J. (1992). Effects of weather on the retrieval of sea ice concentration and ice type from passive microwave data. *Int. J. Remote Sens.*, 13(1): 37-54.
- Meier, W. N., and J. S. Stewart (2020). Assessment of the stability of passive microwave brightness temperatures for NASA Team sea ice concentration retrievals, *Rem. Sens.*, 12(14), 2197. doi: 10.3390/rs12142197.
- Meier, W. N., and J. S. Stewart (2019). Assessing uncertainties in sea ice extent climate indicators, *Env. Res. Letters*, 14, 035005. doi: 10.1088/1748-9326/aaf52c.

- Meier, W.N., J.S. Stewart, Y. Liu, J. Key, and J. A. Miller. (2017). An operational implementation of sea ice concentration estimates from the AMSR2 sensor. *IEEE J. Sel. Topics Appl. Earth Obs. & Rem. Sens.* 10(9) doi: 10.1109/JSTARS.2017.2693120.
- Meier, W.N., G. Peng, D.J. Scott, M.H. Savoie (2014). Verification of a new NOAA/NSIDC passive microwave sea-ice concentration climate record, *Polar Research*, 33, doi:/10.3402/polar.v33.21004.
- Meier, W.N., and S.J.S. Khalsa (2011). Intersensor calibration between F-13 SSM/I and F-17 SSMIS Near-Real-Time Sea Ice Estimates. *Geoscience and Remote Sensing* 49(9): 3343-3349.
- Meier, W.N. (2005). Comparison of passive microwave ice concentration algorithm retrievals with AVHRR imagery in Arctic peripheral seas. *IEEE Trans. Geosci. Remote Sens.*, 43(6): 1324-1337.
- Meier, W.N., T. Maksym, and M. Van Woert (2003). Evaluation of Arctic operational passive microwave products: A case study in the Barents Sea during October 2001. "Ice in Environment: Proceedings of the 16th International Association of Hydraulic Engineering and Research", Dunedin, NZ, 2-6 Dec. 2002, vol. 3:213-222.
- Meier, W.N., M. Van Woert, and C. Bertioia (2001). Evaluation of operational SSM/I ice concentration algorithms. *Ann. Glaciol.*, 33: 102-108.
- Nakagawa, K. (2010). Global Change Observation Mission (GCOM). International Archives of the Photogrammetry, Remote Sensing and Spatial Information Science, Volume XXXVIII.
- NAS (2004). Climate data records from environmental satellites: Interim report, National Academies of Science (NAS), National Academies Press, Washington, D.C., 150 pp.
- Oelke, C. (1997). Atmospheric signatures in sea-ice concentration estimates from passive microwaves: Modelled and observed. *Int. J. Remote Sens.*, 18(5): 1113-1136.
- Ozsoy-Cicek, B., H. Xie, S.F. Ackley, and K. Ye (2009). Antarctic summer ice concentrations and extent: Comparison of ODEN 2006 ship observations and NIC sea ice charts. *The Cryosphere*, 3: 1-9.
- Ozsoy-Cicek, B., S.F. Ackley, A. Worby, H. Xie, and J. Lieser (2011). Antarctic sea-ice extents and concentrations: Comparison of satellite and ship measurements from International Polar Year cruises. *Ann. Glaciol.*, 52(57): 318-326.
- Partington, K.C. (2000). A data fusion algorithm for mapping sea-ice concentrations from Special Sensor Microwave/Imager data. *IEEE Trans. Geosci. Remote Sens.*, 38(4): 1947-1958.

- Peng, G., W.N. Meier, D.J. Scott, and M.H. Savoie (2013). A long-term and reproducible passive microwave sea ice concentration data record for climate studies and monitoring, *Earth Sys. Sci. Data*, 5, 311-318, doi:10.5194/essd-5-311-2013.
- Scambos, T. A., J. A. Bohlander, C. A. Shuman, and P. Skvarca (2004). Glacier acceleration and thinning after ice shelf collapse in the Larsen B embayment, Antarctica. *Geophysical Research Letters*. doi:10.1029/2004GL020670.
- Smith, D.M. (1998). Observation of perennial Arctic sea ice melt and freeze-up using passive microwave data, *J. Geophys. Res.*, 103(C12), 27753-27769.
- Spreen, G., L. Kaleschke, and G. Heygster (2008). Sea ice remote sensing using AMSR-E 89-GHz channels, *J. Geophys. Res.*, 113, C02S03, doi:10.1029/2005JC003384.
- Steffen, K., J. Key, D.J. Cavalieri, J. Comiso, P. Gloersen, K. St. Germain, and I. Rubinstein (1992). The estimation of geophysical parameters using passive microwave algorithms, in "Microwave Remote Sensing of Sea Ice." F.D. Carsey, ed., *American Geophysical Union Monograph* 68, Washington, DC:201-231.
- Wentz F. J. (1997). A well-calibrated ocean algorithm for SSM/I. *J. Geophys. Res.*, 102(C4): 8703-8718.
- Willmes, S., C. Haas, M. Nicolaus, and J. Bareiss (2009). Satellite microwave observations of the interannual variability of snowmelt on sea ice in the Southern Ocean. *J. Geophys. Res.*, 114, C03006, doi:10.1029/2008JC004919.
- Zwally, H.J., J.C. Comiso, C.L. Parkinson, W.J. Campbell, F.D. Carsey, and P. Gloersen (1983). Antarctic sea ice 1973-1976 from satellite passive microwave observations. *NASA Spec. Publ.*, 459, 206 pp.

Appendix A - ACRONYMS AND ABBREVIATIONS

Acronym or Abbreviation	Meaning
AMSR-E	Advanced Microwave Scanning Radiometer for EOS
AMSR2	Advanced Microwave Scanning Radiometer 2
BT	Bootstrap
CATBD	Climate Algorithm Theoretical Basis Document
CDR	Climate Data Record
CLASS	Comprehensive Large Array-data Stewardship System
DAAC	Distributed Active Archive Center
DMSP	Defense Meteorological Satellite Program
DOY	Day of Year
ECDR	Enhanced Climate Data Record
IFOV	Instantaneous Field of View
FY	First Year
GSFC	Goddard Space Flight Center
H	Horizontal
ICDR	Interim Climate Data Record
MY	Multi-year
NAS	National Academies of Science
NASA	National Aeronautics and Space Administration
NCEI	National Center for Environmental Information
NOAA	National Oceanic and Atmospheres Administration
NSIDC	National Snow and Ice Data Center
NRT	Near Real Time
NT	NASA Team
OW	Open Water
QC	Quality Control
RSS	Remote Sensing Systems, Inc.
SMMR	Scanning Multichannel Microwave Radiometer
SSM/I	Special Sensor Microwave Imager
SSMIS	Special Sensor Microwave Imager/Sounder
SST	Sea Surface Temperature
TCDR	Thematic Climate Data Record
V	Vertical